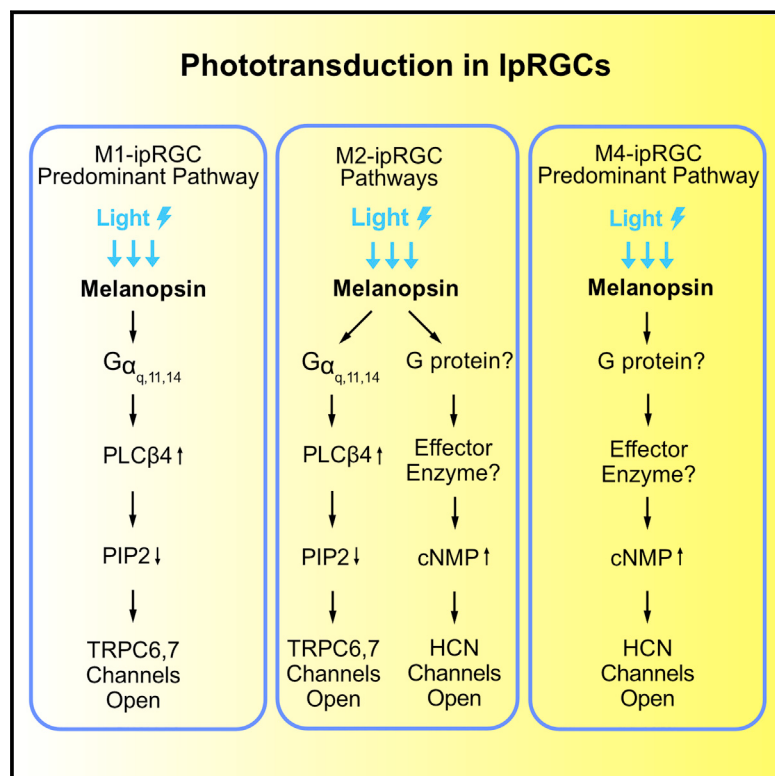


Cyclic-Nucleotide- and HCN-Channel-Mediated Phototransduction in Intrinsically Photosensitive Retinal Ganglion Cells

Graphical Abstract



Authors

Zheng Jiang, Wendy W.S. Yue,
Lujing Chen, Yanghui Sheng,
King-Wai Yau

Correspondence

zjiang314@gmail.com (Z.J.),
kwyau@jhmi.edu (K.-W.Y.)

In Brief

Discovery in retinal ganglion cells of a ciliary phototransduction pathway that uses cyclic nucleotide as the second messenger and HCN as the effector ion channel has evolutionary implications.

Highlights

- Rhabdomeric and ciliary phototransductions coexist in the same cell for some ipRGCs
- Unique among photoreceptor types, basic transduction traits vary in ipRGC subtypes
- IpRGCs use HCN instead of CNG channels for ciliary phototransduction
- The self-regulating property of HCN channels may be important for ipRGC signaling



Cyclic-Nucleotide- and HCN-Channel-Mediated Phototransduction in Intrinsically Photosensitive Retinal Ganglion Cells

Zheng Jiang,^{1,3,*} Wendy W.S. Yue,^{1,3,4,6,7} Lujing Chen,^{1,3,5,6} Yanghui Sheng,^{1,3,5} and King-Wai Yau^{1,2,3,8,*}

¹Solomon H. Snyder Department of Neuroscience, Johns Hopkins University School of Medicine, Baltimore, MD 21205, USA

²Department of Ophthalmology, Johns Hopkins University School of Medicine, Baltimore, MD 21205, USA

³Center for Sensory Biology, Johns Hopkins University School of Medicine, Baltimore, MD 21205, USA

⁴Biochemistry, Cellular and Molecular Biology Graduate Program, Johns Hopkins University School of Medicine, Baltimore, MD 21205, USA

⁵Neuroscience Graduate Program, Johns Hopkins University School of Medicine, Baltimore, MD 21205, USA

⁶These authors contributed equally

⁷Present address: Department of Physiology, University of California, San Francisco, CA 94158, USA

⁸Lead Contact

*Correspondence: zjiang314@gmail.com (Z.J.), kwyau@jhmi.edu (K.-W.Y.)

<https://doi.org/10.1016/j.cell.2018.08.055>

SUMMARY

Non-image-forming vision in mammals is mediated primarily by melanopsin-expressing, intrinsically photosensitive retinal ganglion cells (ipRGCs). In mouse M1-ipRGCs, by far the best-studied subtype, melanopsin activates PLC β 4 (phospholipase C- β 4) to open TRPC6,7 channels, mechanistically similar to phototransduction in fly rhabdomeric (microvillous) photoreceptors. We report here that, surprisingly, mouse M4-ipRGCs rely on a different and hitherto undescribed melanopsin-driven, ciliary phototransduction mechanism involving cyclic nucleotide as the second messenger and HCN channels rather than CNG channels as the ion channel for phototransduction. Even more surprisingly, within an individual mouse M2-ipRGC, this HCN-channel-dependent, ciliary phototransduction pathway operates in parallel with the TRPC6,7-dependent rhabdomeric pathway. These findings reveal a complex heterogeneity in phototransduction among ipRGCs and, more importantly, break a general dogma about segregation of the two phototransduction motifs, likely with strong evolutionary implications.

INTRODUCTION

Intrinsically photosensitive retinal ganglion cells (ipRGCs) are the principal retinal neurons in the mammalian eye sending output signals to the brain for driving non-image-forming visual functions, such as circadian photoentrainment and pupillary light reflex (Berson et al., 2002; Hattar et al., 2002; for reviews, see Do and Yau, 2010; Hatori and Panda, 2010; Hughes et al., 2016; Lucas, 2013; Sand et al., 2012; Schmidt et al., 2011). These photoreceptors fall into several subtypes, M1 through M5, which differ in sensitivity, saturated photocurrent amplitude,

dendritic morphology, and stratification in the retina, as well as projection targets in the brain (see above reviews). They share the same visual pigment, melanopsin (OPN4), which, interestingly, is phylogenetically closer to invertebrate than vertebrate visual pigments (Koyanagi et al., 2005; Provencio et al., 1998).

Unlike the great majority of photoreceptor cells in the animal kingdom, ipRGCs do not show a morphologically distinct cellular compartment containing the visual pigment and the associated signaling components for phototransduction. Photoreceptors generally do have this specialized photosensitive structure and, as such, are classified as being either rhabdomeric (microvillous) or ciliary, depending on whether the structure is microvilli- or cilium-derived (Arendt, 2003; Lamb et al., 2007; Yau and Hardie, 2009). Most invertebrate photoreceptors, such as in *Drosophila* eye, are rhabdomeric. Their phototransduction mechanisms, although often varied in details, conform to the “rhabdomeric” mechanistic motif by involving PLC-mediated signaling. In contrast, vertebrate rods and cones in the lateral eyes and photoreceptors in the lizard parietal eye are all ciliary photoreceptors, conforming to the “ciliary” motif of phototransduction by involving cyclic-nucleotide-mediated signaling (Yau and Hardie, 2009). IpRGCs show no sign of microvilli or cilia, thus offering no structural clue regarding phototransduction. However, possibly in keeping with melanopsin’s closer phylogenetic homology to invertebrate photopigments, M1-ipRGCs turn out to use a rhabdomeric phototransduction motif (Graham et al., 2008; Xue et al., 2011). Specifically, their phototransduction process goes through PLC β 4 and TRPC6 and 7 channels (Xue et al., 2011). In fact, PLC β 4 is the closest vertebrate homolog of the *Drosophila* eye’s PLC, NORPA (Bloomquist et al., 1988; Jiang et al., 1996), and TRPC channels are close vertebrate homologs of the TRP and TRPL channels mediating phototransduction in fly eye (Venkatachalam and Montell, 2007).

Previous studies (Graham et al., 2008; Xue et al., 2011) have concentrated on phototransduction in M1-cells because this ipRGC subtype gives the largest photoresponses and expresses the highest level of melanopsin based on immunohistochemical and genetic labelings, thus readily identifiable for recordings



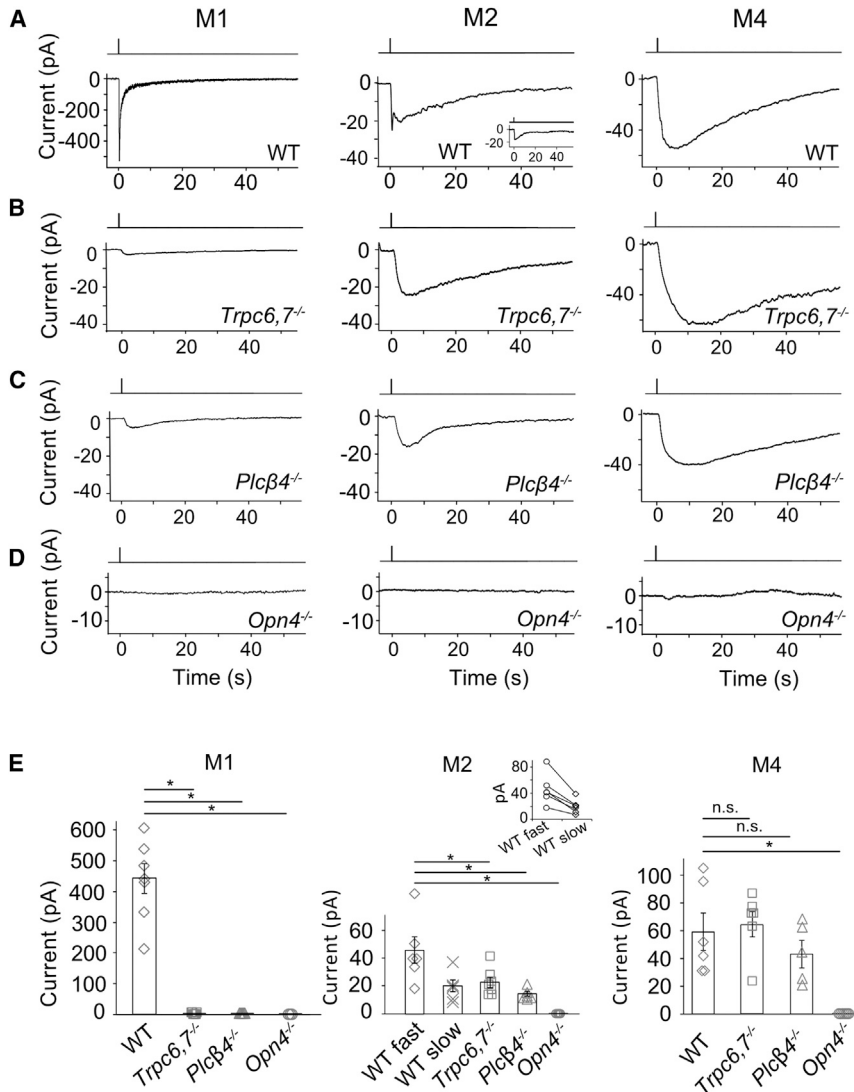


Figure 1. A Phototransduction Mechanism Independent of $\text{PLC}\beta 4$ and $\text{TRPC}6,7$ Exists in ipRGCs

(A–D) Different panels show light responses of M1-, M2-, and M4-cells in flat-mount retinas WT (A), *Trpc6,7*^{-/-} (B), *Plcβ4*^{-/-} (C), and *Opn4*^{-/-} (D) in the presence of synaptic blockers (STAR Methods). Full-field, 200-ms Xe white flash (equivalent to 1.75×10^{10} photons $\mu\text{m}^{-2} \text{s}^{-1}$ of 480-nm light, based on dim-flash-response matching) giving saturated responses in all cases. Cells were targeted based on tdTomato signal in BAC transgenic *Opn4:tdTomato* or *Opn4-Cre;Rosa-tdTomato* retinas (STAR Methods). Voltage-clamp recordings at -66 mV . Single-flash trials in all cases except for *Opn4*^{-/-} (averages of 3 trials).

(E) Averaged data (mean \pm SEM, n = 7, 8, 5, 3; 6, 6, 7, 6, 4; 6, 6, 5, 7 cells from at least 2 animals in each group. *p < 0.05; n.s., not statistically significant. Middle: only 6 out of 9 WT M2-cells showed discrete transient peaks of fast and slow components (shown in inset: each pair connected by straight line); for the remaining 3 cells, only the fast peak was evident (see text and inset of A, middle), thus not included in collected data. For clear visualization, all representative light responses were low-pass filtered at 2 Hz, except for the M1-response in (A), Figures 2B and S2, and the CNGA2-mediated current in Figure 3C, which were low-pass filtered at 20 Hz in order to capture the fast response.

See also Figure S1.

(Do et al., 2009; Emanuel and Do, 2015; Emanuel et al., 2017; Milner and Do, 2017). Photoreceptors within a given type in the animal kingdom are generally found to employ the same phototransduction mechanism, with no indication of distinct mechanisms between different subtypes. In the course of our investigation, however, it has become clear that this is far from true. We report here surprising findings from M2- and M4-cells, two other ipRGC subtypes targetable for live recordings. A key lesson is that a photopigment apparently can signal through both rhabdomeric and ciliary phototransduction motifs in a single photoreceptor cell.

RESULTS



A Second Phototransduction Mechanism in IpRGCs

We performed whole-cell, patch-clamp recordings in flat-mount mouse retina at 30°C – 32°C from ipRGCs labeled genetically by the fluorescent protein, tdTomato (Do et al., 2009; STAR Methods). Initially targeted as M1-, M2-, or M4-ipRGCs based

on fluorescence intensity and soma size, cell identities were confirmed after recording by visualizing dendritic arborizations with the dye, Alexa-568, dialyzed intracellularly from the whole-cell pipette (STAR Methods). Their intrinsic light responses were isolated for study from rod/cone-driven responses by synaptic blockers (STAR Methods). Unless indicated otherwise, light stimulation employed wide-field, 200-ms white flashes eliciting saturated intrinsic responses.

In the genetic background of *Trpc6,7*^{-/-} (short for *Trpc6*^{-/-}; *Trpc7*^{-/-} double-knockout [KO]), the M1-ipRGC's intrinsic light response disappeared almost completely (Figures 1A, 1B, and 1E, left), consistent with previous work (Xue et al., 2011). The wild-type (WT) M2-response typically showed fast and slow components (Figures 1A and 1E, middle), although the slow peak was not always separately visible (inset in Figure 1A, middle, and legend in Figure 1E, middle). Surprisingly, *Trpc6,7*^{-/-} M2-ipRGCs lost only the fast component (Figures 1A, 1B, and 1E, middle), whereas *Trpc6,7*^{-/-} M4-responses showed little change from WT (Figures 1A, 1B, and 1E, right). Ablating $\text{PLC}\beta 4$ gave similar phenotypes as *Trpc6,7*^{-/-} in the three ipRGC subtypes (Figures 1C and 1E). Thus, mouse $\text{TRPC}6,7$ -mediated phototransduction is predominant in M1-cells, but constitutes only a (variable) part of the M2-response and seemingly little of the M4-response. Although minuscule, the residual responses in *Trpc6,7*^{-/-} or

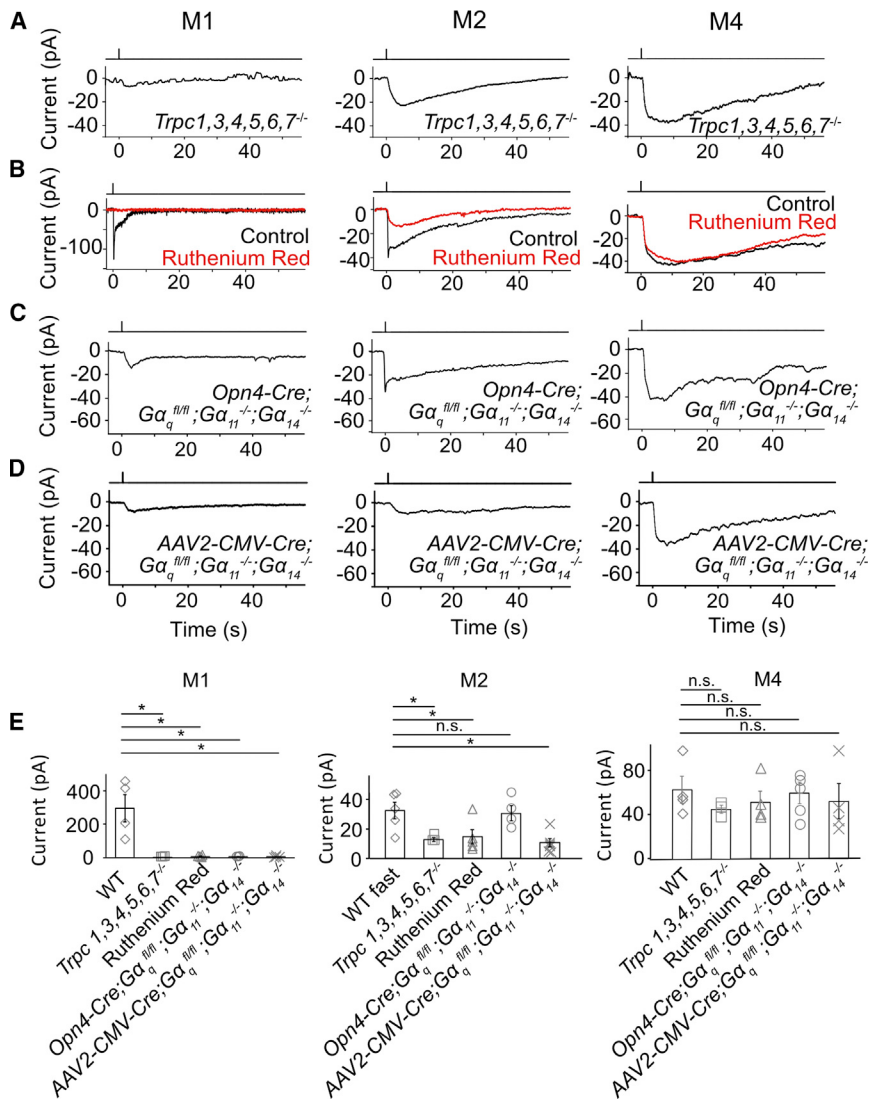


Figure 2. The Unknown Phototransduction Pathway Is Independent of TRPC and G α_q Family Members

(A-D) Saturated light responses of M1-, M2-, and M4-cells of *Trpc1,3,4,5,6,7^{-/-}* (A), WT with 20-μM ruthenium red (B), *Opn4-Cre; Gα_q^{fl/fl}; Gα₁₁^{-/-}; Gα₁₄^{-/-}* (C), and *AAV2-CMV-Cre; Gα_q^{fl/fl}; Gα₁₁^{-/-}; Gα₁₄^{-/-}* (D). Light stimulation and recording condition are the same as in Figure 1.

(E) Averaged data (mean ± SEM, n = 4, 3, 4, 3, 4; 5, 3, 5, 4, 6; 4, 3, 4, 5, 4 cells from at least 2 animals in each group). *p < 0.05; n.s., not statistically significant.

Note that, in (B) middle, the apparent reduction in the slow component of the M2-response by ruthenium red represents actually the removal of the slow decline of the fast component; indeed, ruthenium red showed no effect on *Trpc6,7^{-/-}* M2-cells (not shown). In (C) left, 3 out of 5 *Opn4-Cre; Gα_q^{fl/fl}; Gα₁₁^{-/-}; Gα₁₄^{-/-}* M1-ipRGCs had a very small residual response, but the remaining two M1-cells gave a normal-looking response (not shown and not included in E left); in (C) middle and right, the *Opn4-Cre; Gα_q^{fl/fl}; Gα₁₁^{-/-}; Gα₁₄^{-/-}* M2- and M4-ipRGC also appeared normal, probably due to weak *Opn4* promoter and thus Cre-recombinase activity (see text). In (D), 4 out of 4 *AAV2-CMV-Cre*-infected M1-ipRGCs showing GFP-fluorescence (thus indicating successful infection) had a small residual response, 6 out of 6 infected M2-ipRGCs showing GFP-fluorescence lost the fast response component, and 4 out of 4 M4-ipRGCs showing GFP-fluorescence had normal-looking responses. The indicated WT cells were actually those used in the ruthenium red experiments but before ruthenium red application (thus distinct from those indicated from those in Figure 1E, although giving similar photocurrents).

See also Figures S1 and S2.

Plc β 4^{-/-} M1-ipRGCs likely reflect a small presence also in M1-cells of non-TRPC6,7-mediated phototransduction (see later). Regardless of M1-, M2-, or M4-cells, the light response disappeared in *Opn4^{-/-}* background (Figures 1D and 1E, indicating melanopsin's involvement throughout).

The unknown phototransduction pathway in M2- and M4-cells does not simply use other PLC β or TRPC isoforms. Thus, *Plc β 1^{-/-}*, *Plc β 2^{-/-}*, and *Plc β 3^{-/-}* genotypes had no effect (Figure S1), and *Trpc1,3,4,5,6,7^{-/-}* and *Trpc6,7^{-/-}* were similar (Figures 1B, 1E, 2A, and 2E); *Trpc2^{-/-}* was also examined, giving the same result (not shown). We did not check the M4-response in some KO lines above, but it is similar to M2-response's slow component in kinetics, pharmacological properties, and susceptibility to specific genetic manipulations (see below), suggesting their common mechanistic origin. Finally, the wide-spectrum TRP-channel-superfamily blocker, ruthenium red (Meotti et al., 2014), eliminated almost completely the M1-response and the fast component of the M2-response, but did not affect M2-

response's slow component or the M4-response (Figures 2B, 2E, and 2B legend). Thus, the TRP-channel superfamily likely does not partake in the unknown phototransduction pathway.

G Protein

We next asked whether the TRPC6,7-mediated pathway and the unknown pathway bifurcate at the G-protein step. In the TRPC6,7-pathway, the importance of PLC β 4 suggests the G α_q -subfamily's involvement upstream (Graham et al., 2008; Xue et al., 2011). Others have found normal non-image vision in *Opn4^{Cre/+}; Gα_q^{fl/fl}; Gα₁₁^{-/-}* (i.e., conditional double-KO) mice (Chew et al., 2014), although simultaneous RNA-knockdowns of G α_q , G α_{11} , and G α_{14} genes led to partial deficits (Hughes et al., 2015). We similarly found normal-looking M1-responses in several G α_q -subfamily single- and double-KO lines (Figure S2), but severely reduced responses (3 out of 5 M1-cells) in the conditional triple-KO line (*BAC transgenic Opn4-Cre; Gα_q^{fl/fl}; Gα₁₁^{-/-}; Gα₁₄^{-/-}*) (Figures 2C and 2E, left). The other two

M1-cells and most M2-cells with this genotype did not show this effect (Figure 2C, legend), possibly due to low Cre-recombinase expression driven by the weak *Opn4* promoter (Wang et al., 2017). As an alternative approach, we introduced Cre-GFP into $G\alpha_q^{fl/fl};G\alpha_{11}^{-/-};G\alpha_{14}^{-/-}$ mouse eyes via adeno-associated virus serotype 2 (AAV2-CMV-Cre-GFP; STAR Methods). All successfully infected M1-cells as revealed by GFP-fluorescence gave tiny intrinsic responses (Figures 2D and 2E, left; STAR Methods). More importantly, similarly treated M2-cells uniformly lost the fast but not the slow response component (Figures 2D and 2E, middle), whereas M4-responses remained largely unchanged (Figures 2D and 2E, right).

In summary, $G\alpha_q$, $G\alpha_{11}$, and $G\alpha_{14}$ mediate the TRPC6,7-pathway with redundancy, but a G-protein of another subfamily or even $G\beta\gamma$ may mediate the second phototransduction pathway (Bailes and Lucas, 2013).

Involvement of Cyclic Nucleotide but Not Cyclic-Nucleotide-Gated Channel

As mentioned in the Introduction, photoreceptors in the animal kingdom are typically either microvillous (rhabdomeric) or ciliary in morphology, employing correspondingly a PLC-mediated or a cyclic-nucleotide-mediated mechanistic motif for phototransduction (Arendt, 2003; Yau and Hardie, 2009). Given that the unknown pathway in M2- and M4-cells is independent of PLC, we checked the cyclic-nucleotide motif. We dialyzed 50- μ M BCMCM-cyclic adenosine monophosphate (cAMP) or BCMCM-cyclic guanosine monophosphate (cGMP) (caged-cAMP or -cGMP compound) into an ipRGC of *Opn4^{-/-}* retina from the whole-cell pipette (STAR Methods). Photo-uncaging cAMP in primarily the soma gave almost no current in M1-cells ($n = 3$ cells from 2 animals), versus a small inward current in M2-cells (3.3 ± 1.2 pA, mean \pm SEM, $n = 4$ cells from 3 animals) and a larger current in M4-cells (17.9 ± 5.1 pA, $n = 4$ cells from 2 animals) (Figure 3A, top). Photo-uncaging cGMP at the same light intensity elicited no detectable current in M1- and M2-cells ($n = 4$ cells in each group from 2 and 3 animals, respectively) but a small current in M4-cells (5.6 ± 1.2 pA, $n = 4$ cells from 3 animals) (Figure 3A, bottom). Control photo-stimulation without caged compound elicited no responses ($n = 3$ cells from 2 animals for each cell type). As such, the currents elicited by uncaged cAMP or cGMP across *Opn4^{-/-}* M1-, M2-, and M4-cells paralleled qualitatively the respective *Trpc6,7^{-/-}* intrinsic light responses (i.e., via the unknown pathway; see Figure 1B) in relative amplitudes and also in their slow kinetics. The quantum efficiency of BCMCM-cAMP (0.10) is lower than that of BCMCM-cGMP (0.14) (Givens et al., 2003), yet the current elicited by uncaged cAMP is larger. Thus, the cyclic nucleotide-sensitive entity in these cells is more sensitive to cAMP than to cGMP.

Vertebrate rod/cone phototransductions and main olfactory transduction all employ cyclic-nucleotide-gated (CNG), non-selective cation channels (Biel and Michalakis, 2009; Kaupp and Seifert, 2002). We thus checked the potential presence of such channel subunits (CNGA1-4, CNGB1, and CNGB3) in ipRGCs by immunohistochemistry (STAR Methods). However, we did not detect any CNG-channel immunosignal co-localized with melanopsin-promoter activity in *Opn4-Cre;Rosa-tdTomato*

(Ai9) mouse retina (Figure 3B, top) (Warren et al., 2006), despite positive controls for the antibodies' specificities (Figure 3B, bottom). Importantly, CNG channels are generally more sensitive to cGMP than to cAMP (Biel and Michalakis, 2009; Kaupp and Seifert, 2002), unlike our finding above with photo-uncaged cyclic nucleotides. Thus, CNG channels are unlikely to be involved in M2- and M4-phototransduction.

Although extrinsically introduced cyclic nucleotide in *Opn4^{-/-}* M2- and M4-cells gave an inward current resembling the intrinsic light response, the question remains whether their native phototransduction elevates cyclic nucleotide. Although CNG channels are not in ipRGCs, we can use them as a cyclic-nucleotide sensor by heterologous expression via virus in *Trpc6,7^{-/-}* ipRGCs. These much-studied channels are known to be opened by, and only by, cyclic nucleotide with rapid gating (Biel and Michalakis, 2009; Kaupp and Seifert, 2002). We chose the key olfactory CNG channel subunit, CNGA2, for this purpose based on its highest sensitivity to cyclic nucleotide (Biel et al., 2009) (STAR Methods). Indeed, we observed a light-induced, distinct inward current with a fast transient peak in *Trpc6,7^{-/-}* M4-ipRGCs virally infected with CNGA2 (Figure 3C). Thus, native phototransduction does trigger cyclic-nucleotide elevation.

Because CNGA2 is highly sensitive to both cAMP and cGMP, we are unable yet to pinpoint the true second messenger. In favor of cAMP, locally applied forskolin, an adenylyl-cyclase activator, elicited in WT M4-cells a transient inward current, suggesting the presence of this enzyme (Figure S3A, right trace). The forskolin effect was smaller in WT M2-cells, and still smaller in WT M1-cells (Figure S3A, middle and left traces; collected data in Figure S3A, extreme right). The phosphodiesterase inhibitor, IBMX, also elicited a transient inward current, with a gradation of amplitudes across the WT ipRGC subtypes similar to that triggered by forskolin, suggesting a correlated co-presence of the cyclic-nucleotide hydrolytic enzyme (Figure S3B). Finally, the adenylyl-cyclase inhibitor, ST034307, significantly blocked the *Trpc6,7^{-/-}* M4-intrinsic light response, possibly suggesting the enzyme being also in the phototransduction pathway (Figure S3C, left and far right). However, the soluble-guanylate-cyclase inhibitor, LY83583, surprisingly also blocked the light response (Figure S3C, middle and far right), not fitting the cAMP picture (see Discussion). The LY83583 effect is possibly non-specific, but needs future scrutiny.

In short, the notion of the second phototransduction pathway involving a rise in cyclic nucleotide is conclusive, but the more detailed question regarding the second messenger being cAMP or cGMP remains somewhat open.

Involvement of an HCN-Channel

With CNG channels not involved, we turned to HCN channels, which are cation channels opened by cyclic nucleotide and also by membrane hyperpolarization (hence "HCN") (Biel et al., 2009). These channels give rise to the I_h current underlying the pacemaking of cardiac muscle cells' membrane potential (DiFrancesco, 1993) and are found in many rat RGCs (Chen and Yang, 2007; Van Hook and Berson, 2010; Lee and Ishida, 2007), including ipRGCs (Van Hook and Berson, 2010). As a quick check, we applied the HCN-channel blocker, ZD7288 (Van Hook and Berson, 2010; Lee and Ishida, 2007) and found

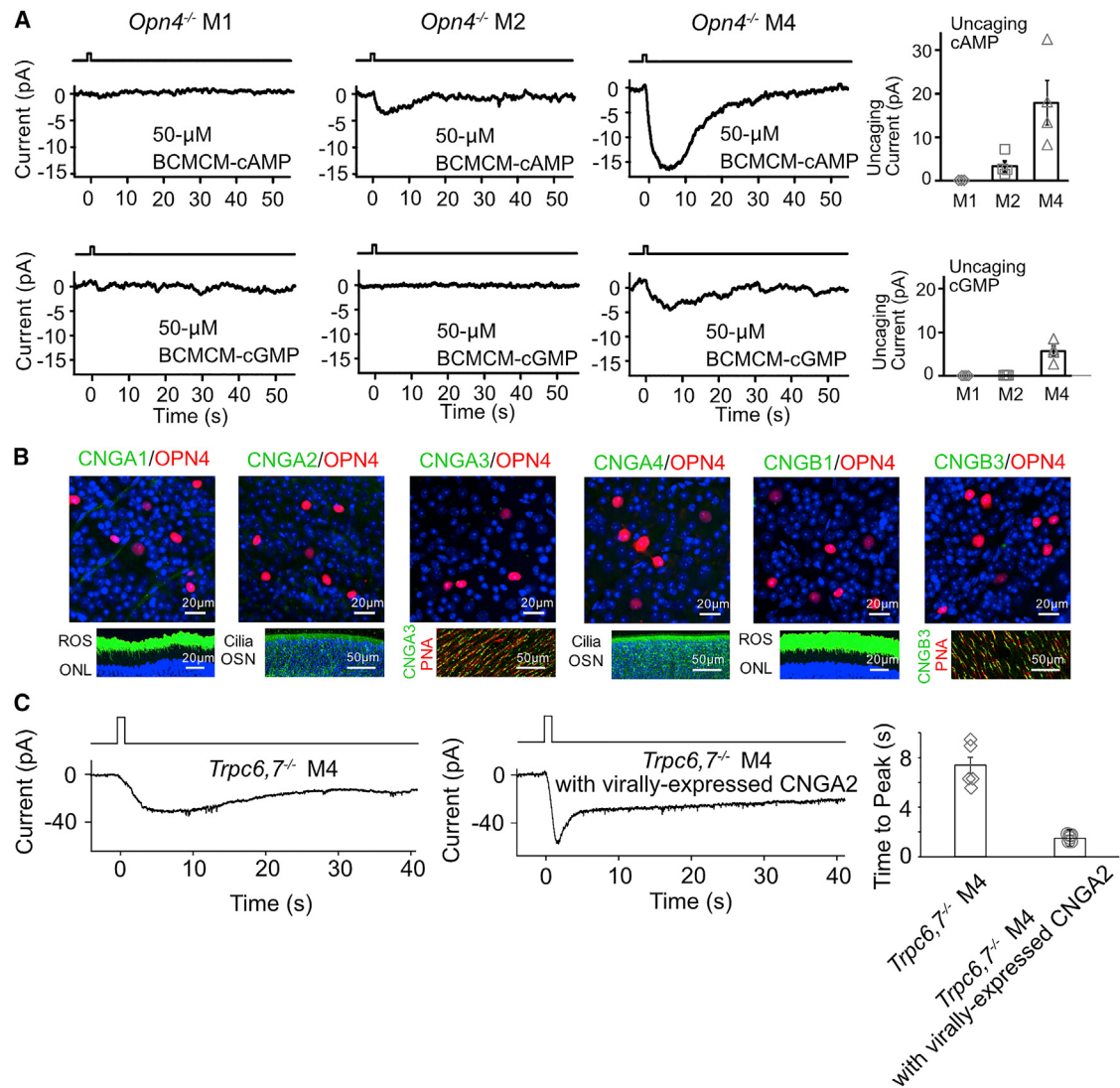


Figure 3. IpRGCs Express Ion Channels Regulated by Cyclic Nucleotide and Produce Cyclic Nucleotide in Phototransduction

(A) *Odn4*^{-/-} genotype. Voltage-clamp recordings at -66 mV. Left 6 panels: inward currents elicited by photo-uncaged cAMP or cGMP in M1-, M2-, and M4-cells. 50- μ M BCMCM-cAMP or -cGMP was loaded into the recorded cell via the whole-cell pipette. Photo-uncaging achieved by white-light spot (Hg lamp, 1 s, 0.12 μ W μ m $^{-2}$, 40 μ m in diameter) centered on recorded soma. Far right: collected data (mean \pm SEM, n = 3, 4, 4 cells at top and 4, 4, 4 cells at bottom from at least 2 animals in each group; see text).

(B) Top: lack of immunosignals for various CNGA- and CNGB-subunits (STAR Methods) in RGC layer of flat-mount *Odn4-Cre; Rosa-tdTomato* retina (red, tdTomato indicating ipRGCs; green, respective CNG channel but not detected). Bottom: verification of positive immunostaining (green) with the same CNG-antibodies for rods and cones as well as olfactory sensory neurons. Retinal cross-sections for CNGA1 and CNGB1; ROS, rod outer segment; ONL, outer nuclear layer. Main olfactory epithelial cross-sections for CNGA2 and CNGA4; OSN, olfactory sensory neurons with cilia. Flat-mount retinas for CNGA3 and CNGB3; cone outer segments marked by peanut agglutinin (PNA, red). Blue color is DAPI nuclear staining.

(C) *Trpc6,7*^{-/-} M4-ipRGC with virally expressed CNGA2 subunit (middle) has a light response with a faster rising phase compared to non-infected cell (left), indicating that cyclic nucleotide is produced in the unknown phototransduction pathway. The duration of light stimulation was 1 s. Right: collected data of time to peak, mean \pm SEM, n = 5, 6 cells from at least 2 animals in each group.

See also Figure S3.

it (at 50 μ M) to literally abolish the *Trpc6,7*^{-/-} residual intrinsic M2-response (Figure 4A), as well as the *Trpc6,7*^{-/-} tiny residual M1- and entire M4-responses (Figure S4A). The small residual M2- and M4-response in ZD7288 (collected data in Figure S4B) may come from incomplete penetration of ZD7288 through the retina, or possibly yet another channel.

We checked whether the channels underlying the light response also had the unusual HCN-channel property of being hyperpolarization-activated (Biel et al., 2009). Indeed, when the cell was hyperpolarized from -66 mV to -96 mV, the *Trpc6,7*^{-/-} M2-response decreased to approximately half (Figure 4B; mean \pm SEM = 39.1% \pm 9.8%, n = 5 cells from 2 animals). This

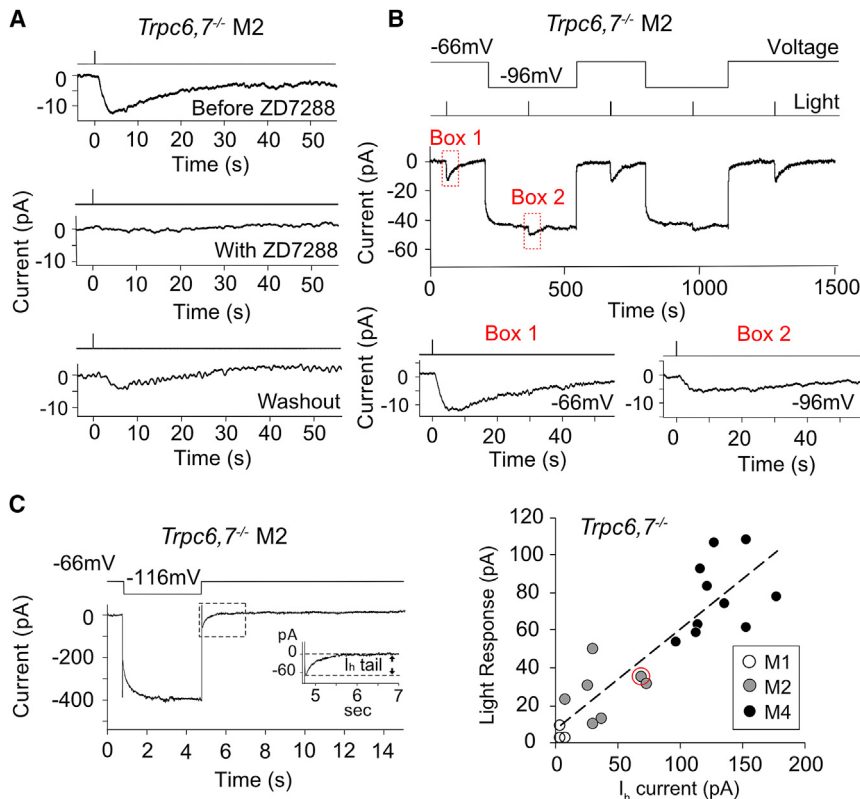


Figure 4. Pharmacological and Physiological Evidence Suggest HCN Channel Is Involved in M2- and M4-Phototransductions

(A) *Trpc6,7^{-/-}* M2-response was fully blocked by bath-applied ZD7288 (50 μ M), an HCN-channel blocker, with partial recovery during washout. See corresponding experiments on *Trpc6,7^{-/-}* M1- and M4-responses, as well as all collected data in Figure S4.

(B) Top: membrane hyperpolarization reduced the light response of *Trpc6,7^{-/-}* M2-cell. Saturated light response was reduced to $39.1\% \pm 9.8\%$ (mean \pm SEM, $n = 5$ cells from 2 animals) of WT when cell was hyperpolarized from -66 mV to -96 mV. Bottom: boxed traces magnified.

(C) Left: I_h tail current of a *Trpc6,7^{-/-}* M2-cell induced by a 4-s hyperpolarization to -116 mV before returning to -66 mV. Inset: boxed trace magnified. Right: collective plot across M1-, M2-, and M4-cells showing a roughly linear relation between light response (at -66 mV) and I_h tail current amplitudes of *Trpc6,7^{-/-}* ipRGCs; the data point circled in red corresponds to the specific experiment on left. These datasets are distinct from those shown in Figure 1; unlike Figure 1, both I_h current and light response are measured for each cell here. Linear regression line: $y = 0.52x + 7.19$, $R^2 = 0.76$.

See also Figure S4.

observation is consistent with the notion that more HCN channels became open during hyperpolarization in darkness to leave fewer channels for opening upon illumination. Furthermore, the saturated intrinsic light response across *Trpc6,7^{-/-}* M2- and M4-ipRGCs (at -66 mV) was roughly proportional in amplitude to a given cell's I_h tail current (also at -66 mV) assayed immediately after a membrane hyperpolarization to -116 mV, with little current shown by M1-cells (Figure 4C, right). Finally, HCN channels are more sensitive to cAMP than cGMP (Biel et al., 2009), in line with the stronger uncaged-cAMP effect found above.

Among HCN channels, HCN2 and HCN4 show strong cyclic-nucleotide sensitivity, whereas HCN1 and HCN3 show weak or no apparent sensitivity (Biel et al., 2009). *Hcn1^{-/-}* and *Hcn2^{-/-}* genotypes did not remove M2-cells' I_h tail current (Figures S5A, S5B, and S5E), but this does not rule out their presence because native HCN channels are tetramers and can be heteromeric. *Hcn4^{-/-}* is embryonic-lethal (Stieber et al., 2003), so we examined *Opn4-Cre;Hcn4^{fl/fl}* M2 cells but found little effect on the I_h tail current (Figures S5C and S5E). The same was found with AAV2-CMV-Cre-GFP; *Hcn4^{fl/fl}* M2 cells, probably due to great difficulty presented by the *Hcn4^{fl/fl}* line for Cre-recombinase action as previously reported (Herrmann et al., 2007). Not giving up, we made an attempt with a pan-retina Cre (Six3-Cre), with further improvement by using the heterozygous *Hcn4^{fl/fl}* instead of homozygous *Hcn4^{fl/fl}* (i.e., one *Hcn4* allele is already constitutively ablated) and by including *Hcn2^{-/-}* to hopefully ablate *Hcn2* and *Hcn4* simultaneously. Unfortunately, we still failed to remove the I_h tail current (Figures S5D

and S5E). As an alternative, we took a dominant-negative approach with a mutant HCN channel subunit via AAV2 virus (see Figure 5A for AAV plasmid). We used a mutant HCN2 (mut-HCN2; HCN4 cDNA is too long to fit easily in AAV2) with a disrupted pore region for preventing cation conduction (Xue et al., 2002) and fused it to a V5 tag for detecting mut-HCN2 expression by immunohistochemistry. HCN2 is capable of forming homo-tetramers and hetero-tetramers at least with HCN4 (Biel et al., 2009). In HEK293 cells, mut-HCN2 largely removed the I_h current going through heterologously expressed HCN4 (Figure 5B), thus validating a dominant-negative effect. We then co-injected a mixture of AAV2-CMV-GFP (for tracking viral infection) and AAV2-mut-HCN2 into eyes of *Trpc6,7^{-/-}* animals (Figure 5C), and found that 80% of GFP-positive M2-cells recorded ($n = 15$ cells from 9 animals) and 85% of GFP-positive M4-cells recorded ($n = 13$ cells from 6 animals) displayed a much reduced I_h tail current (with the criterion being $<1/3$ of average amplitude in uninfected cells). These successfully infected M2- and M4-ipRGC sub-populations also showed a concomitant, much reduced light response (Figure 5D, legend; STAR Methods).

In parallel, two antibodies (Mataruga et al., 2007) against mouse HCN4 labeled bipolar cells as positive control but showed no clear specific labeling of mouse ipRGCs, perhaps due to low HCN4 expression. We next tried genetic labeling by using the heterozygous *HCN4nlacZ/H2BGFP* mouse line (stock 024284, Jackson Laboratory), in which one *Hcn4* allele is WT and the other is replaced by *nlacZ/H2BGFP*, which expresses

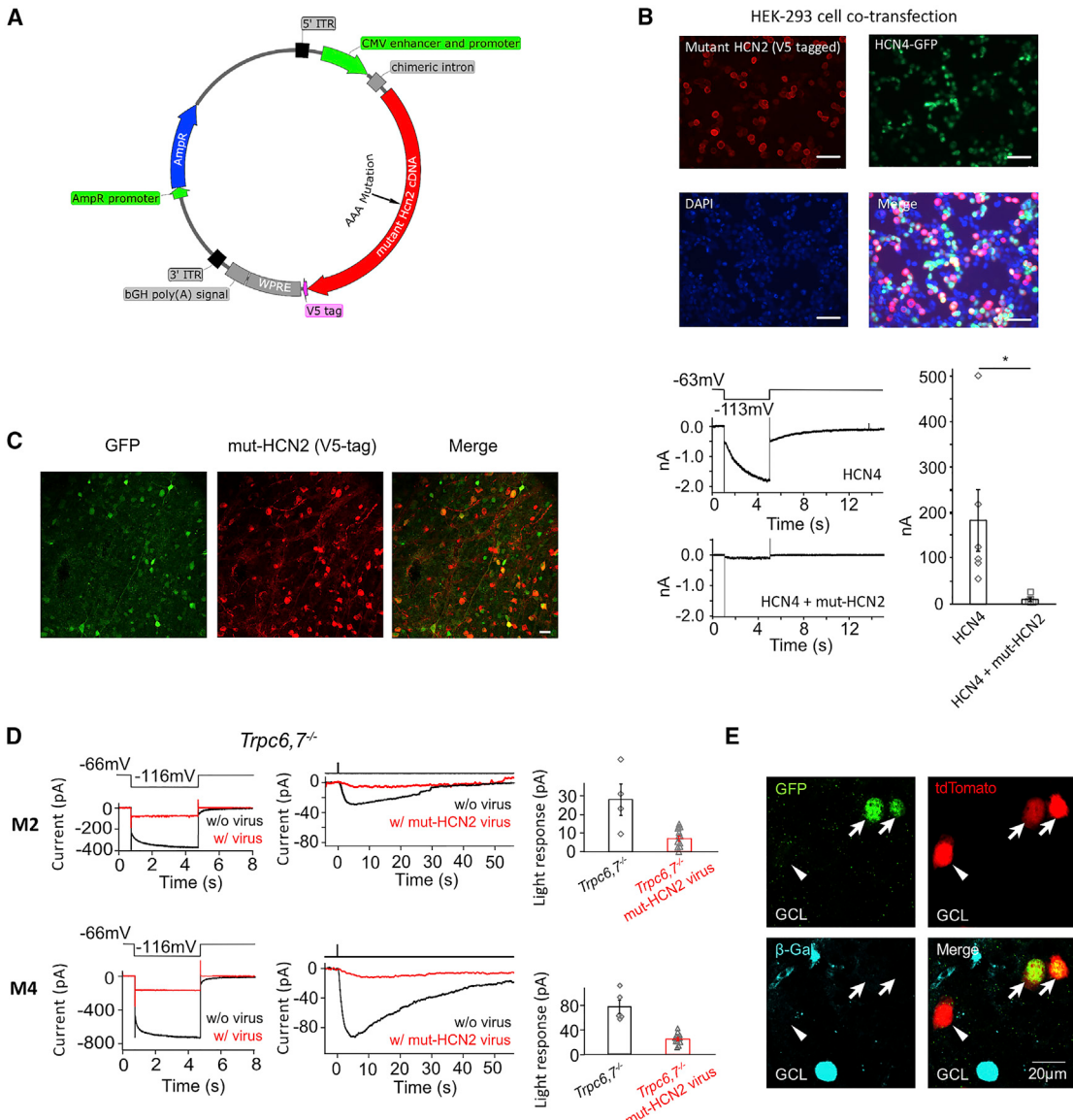


Figure 5. Dominant-Negative Experiment and Genetic Labeling Indicate that HCN Channels Are Involved in M2- and M4-Phototransductions and HCN4 Is Expressed in ipRGCs

(A) AAV plasmid for expressing mutant HCN2 as a dominant-negative HCN-channel subunit in retina. *Hcn2* cDNA was inserted after the CMV enhancer and promoter and was followed by a V5 tag for post hoc identification of successfully transfected/infected cells by immunostaining.

(B) Top: HEK293 cells co-transfected with a mutant *Hcn2* AAV plasmid (including a fused V5-tag) and a WT *Hcn4* plasmid (including a nuclear GFP cDNA in the same plasmid but driven by a separate promoter). Scale bar, 50 μm. Approximately half of the cells were successfully transfected with the *Hcn4* construct (i.e., GFP-positive), out of which 96% were also successfully transfected with the mutant *Hcn2* construct (i.e., immuno-positive for V5-tag). Bottom left: a cell co-transfected with mutant *Hcn2* and WT *Hcn4* plasmids showed a greatly reduced I_h tail current compared to a cell singly transfected with WT *Hcn4* plasmid, indicating successful disruption of HCN4 channel function by mutant HCN2. Bottom right: collective data (mean ± SEM, n = 6 cells for each group).

(C) Infection of mouse retina with a mixture of AAV2-mut-HCN2 and AAV2-CMV-GFP viruses. Two weeks after injection, ~80% of GFP-positive cells in retinal ganglion cell layer were also co-infected by the mutant-HCN2 virus as indicated by immunostaining for the V5-tag. Scale bar, 20 μm.

(D) Dominant-negative experiment on *Trpc6,7^{-/-}* M2-cell (top) and M4-cell (bottom) with AAV2-mut-HCN2 virus. Left: loss of I_h tail current (red) indicates successful dominant-negative disruption of native HCN-channel function in a given cell. Middle: much-reduced light response (red) of the same cell. Right: collective results (mean ± SEM, top, n = 4 and 12 cells from 4 and 9 animals respectively; bottom, n = 5 and 11 cells from 2 and 5 animals respectively, p < 0.05); only those virus-infected M2- and M4-cells that showed an I_h tail current reduced below a certain criterion amplitude (STAR Methods) were included. Uninfected cells were recorded from littermate control mice.

(E) Multiple images of the same location in flat-mount *HCN4nLacZ/H2BGFP;Opn4-Cre;Rosa-tdTomato* (see text) retina to show genetic labeling revealing co-localization of *Opn4* (indicated by red tdTomato signal) and *Hcn4* (indicated by green GFP signal). This co-localization in two cells (arrows) is demonstrated by

(legend continued on next page)

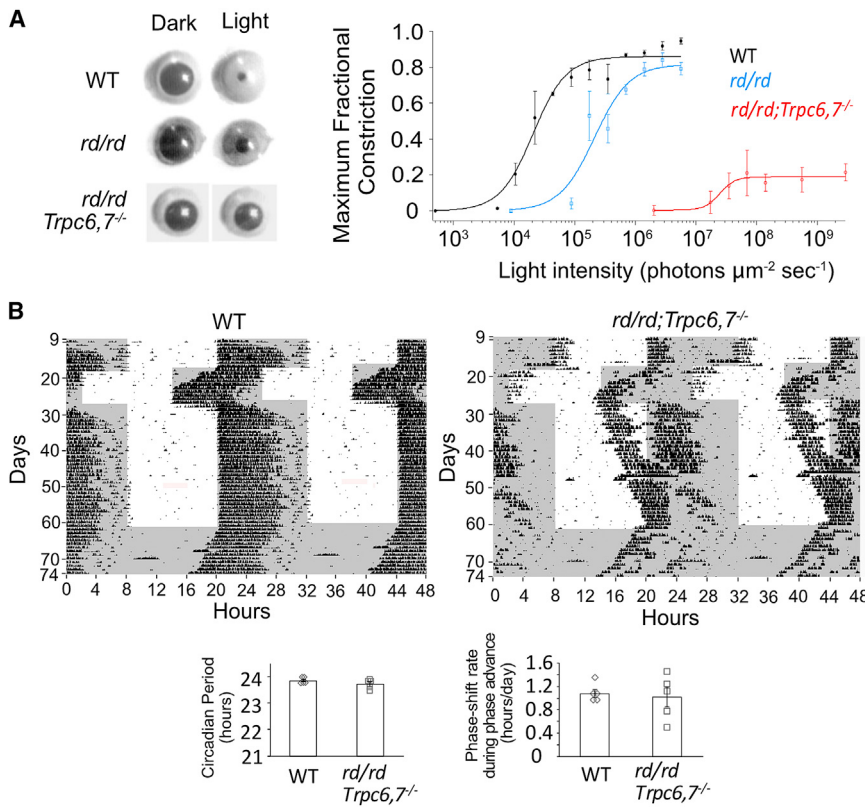


Figure 6. HCN-Channel-Mediated Phototransduction Is Sufficient for Eliciting Behavioral Light Responses

(A) Left: consensual maximum (i.e., at transient peak) PLR elicited by a 1-min light step (505 nm, giving 1.4×10^6 (WT), 5.6×10^6 (rd/rd), and 1.8×10^9 (rd/rd;Trpc6,7^{-/-}) photons $\mu\text{m}^{-2} \text{ s}^{-1}$). Right: collected data (mean \pm SEM) showing relation between light intensity and maximum (i.e., at transient peak) pupillary fractional constriction (MFC) ($n = 3, 3, 5$ animals for WT, rd/rd, and rd/rd;Trpc6,7^{-/-}), with MFC = 1 - (normalized pupil area in light) = 1 - (pupil area in light/pupil area in darkness). Intensity-response relation was fit with Hill equation, $A \times I^{n(H)} / (I^{n(H)} + I_{1/2}^{n(H)})$, with $I_{1/2} = 2.1 \times 10^4$ photons $\mu\text{m}^{-2} \text{ s}^{-1}$, $n(H) = 1.6$ for WT, 2.1×10^5 photons $\mu\text{m}^{-2} \text{ s}^{-1}$, $n(H) = 1.5$ for rd/rd and 2.5×10^7 photons $\mu\text{m}^{-2} \text{ s}^{-1}$, $n(H) = 3.5$ for rd/rd;Trpc6,7^{-/-}.

(B) Top: double-plotted actograms of wheel-running under 12/12 hr L/D cycle, 1,000-lux white light. The rd/rd;Trpc6,7^{-/-} mouse was photo-entrained like WT in response to a 6-hr phase advance in the L/D cycle, but was much more sluggish than WT in adjusting to a 6-hr phase retreat. Shaded region indicates dark condition and vertical blips indicate wheel-running. Bottom: collected data showing periodicity in continuous darkness (WT: 23.85 ± 0.05 hr; mutant: 23.72 ± 0.08 hr, with $n = 5$ animals for each group, mean \pm SEM, $p > 0.05$) and phase-shift rate during 6-hr phase advance (days 18–22) (WT: 1.08 ± 0.07 hr/day; mutant: 1.02 ± 0.17 hr/day, with $n = 5$ animals for each group, mean \pm SEM, $p > 0.05$).

nuclear LacZ in the absence of Cre-recombinase (Figure S6A) but expresses GFP in its presence. As such, upon crossing this line to *Opn4-Cre;Rosa-tdTomato* mice, any ipRGCs (i.e., melanopsin-positive) expressing HCN4 should be co-labeled by GFP and tdTomato. These cells were indeed observed, and appeared to be M2- and M4-cells based on soma size and tdTomato-brightness (Figure 5E, indicated by arrows in all panels and also by yellow color in bottom right panel; see legend). Additionally, there were some tdTomato-positive, GFP-negative cells (arrowhead in Figure 5E). These might include M1-ipRGCs, which have a small I_h current (Figure 4C, right) and thus low HCN4 expression, as well as probably some M2- and M4-cells that failed to turn on GFP-expression due to low *Opn4-Cre* activity. As further confirmation, *in situ* hybridization with the RNAscope 2-Plex assay (STAR Methods) showed partial co-localization of *Hcn4* and *Opn4* mRNA in mouse retinal ganglion cell layer (Figure S6B). The *Opn4*-mRNA clusters with abundant puncta (M1-like cells) usually have few associated *Hcn4* mRNA (e.g., Figure S6B, box X), whereas *Opn4*-mRNA clusters with sparse puncta (M2/M4-like cells) usually have abundant *Hcn4* mRNA in close proximity (e.g., Figure S6B, box Y), consistent with our electrophysiological

data (Figure 4C). A negative-control probe targeting a bacterial gene gave no labeling in the retina (*dapB*, Figure S6C).

All physiological, pharmacological, and molecular biological evidence put together suggests very strongly HCN channels serving as the final effector in the second phototransduction mechanism. However, despite much effort, the molecular identities of the native-channel subunits remain incomplete.

Behavioral Experiments

Can the HCN-mediated phototransduction pathway support non-image vision? We examined the pupillary light reflex (PLR) in rd/rd;Trpc6,7^{-/-} mice (>4 months; STAR Methods), which lose rods and cones due to degeneration (rd/rd) and lack TRPC6,7-mediated phototransduction in ipRGCs, leaving presumably only the HCN-mediated pathway. Consensual PLR (i.e., illuminating one eye and measuring PLR in the other eye) was used in order to avoid the local PLR component from melanopsin in the iris sphincter muscle (Wang et al., 2017; Xue et al., 2011). We did find a residual consensual PLR, although much less sensitive than WT, with rd/rd mice in between (Figure 6A). HCN-mediated phototransduction is also capable of driving circadian photoentrainment by itself, as these mice shifted their wheel-running rhythm (STAR Methods) in

the yellow color in bottom image. Note that the immunosignal (blue) for β -Gal (protein coded by LacZ) was segregated from the tdTomato and GFP signals, indicating *Hcn4* expression in also some conventional (i.e., non-ipRGC) retinal ganglion cells. The GFP-negative, tdTomato-positive cell (indicated by arrowhead) is possibly an M1-ipRGC, which has a low expression of HCN channels (see Figure 4C, right).

See also Figures S5 and S6.

response to a phase advance in the ambient light/dark (L/D) cycle (**Figure 6B**). However, they took much longer than WT to re-adjust to a 6-hr phase delay in the L/D cycle. They also had abnormally long periods of inactivity in darkness.

DISCUSSION

Here, we report the surprising discovery that ipRGCs use the ciliary phototransduction motif, in addition to the rhabdomeric motif involving PLC, both being triggered by melanopsin. **The ciliary motif in ipRGCs involves a rise in cyclic nucleotide and the opening of HCN channels**—the first example of such channels serving as an effector channel in phototransduction.

Not only is the HCN pathway present in M4-ipRGCs, but, even more surprisingly, the TRPC6,7 and HCN pathways co-exist in a given M2-ipRGC, operating in parallel albeit with different kinetics (the HCN pathway being slower). **Both pathways lead to ipRGC excitation through membrane depolarization**. Such a dual-motif mechanism, involving a commingling of rhabdomeric and ciliary pathways in the same cell, is extremely unusual. Strictly speaking, this dual mechanism is not confined to M2-ipRGCs, because the HCN pathway appears to be rudimentarily present in M1-ipRGCs as well. Likewise, a remnant of the TRPC6,7 pathway may exist in M4-ipRGCs, albeit not yet closely examined by us. **The alternative notion that the entire second pathway is an offshoot from the PLC-TRPC6,7 pathway is untenable because the second pathway is independent of Gq-subfamily members, PLC β isoforms, and TRPC channels.**

We shall discuss below the implication of the above finding to a currently exciting question regarding photoreceptor evolution (Arendt et al., 2004, 2009; Feuda et al., 2012; Gehring and Ikeo, 1999; Lamb, 2013; Lamb and Hunt, 2017; Lamb et al., 2009; Shichida and Matsuyama, 2009; Vopalensky et al., 2012). We shall also interpret the potential functional significance of HCN channels used by ipRGCs instead of the canonical CNG channels typically involved in ciliary phototransduction.

Potential Evolutionary Implications of IpRGC Phototransduction

It was suggested (Arendt et al., 2009; Gehring and Ikeo, 1999) that rhabdomeric and ciliary photoreceptors in the animal kingdom may have originated from a single ancestral photoreceptor cell containing both signaling motifs. In extant species examined so far, however, these two motifs are invariably segregated in different photoreceptor types along with their respective r(rhabdomeric)- and c(ciliary)-opsins as inferred from visual-pigment phylogeny. **Situations of more than one pigment per cell do exist (e.g., mouse cones [Applebury et al., 2000] and lizard parietal-eye photoreceptor [Su et al., 2006])**, but the co-existent pigments always share the same phototransduction motif, despite dissimilar details. Most recently, two opsins belonging to two different opsin groups were reported in one cell (Vöcking et al., 2017), but this scenario still differs from a single r-opsin (melanopsin) activating both rhabdomeric and ciliary signaling motifs in one ipRGC. As such, our finding appears to hark back to—and provide evidence for—the above evolutionary proposal by others of an ancestral photoreceptor with both rhabdomeric and ciliary signaling motifs. If so,

evolutionarily the most advanced animals (mammals) also happen to have evolutionarily a most primitive photoreceptor!

The rhabdomeric motif in ipRGCs is highly homologous to that in fly, down to molecular identities. The direct gating mechanism for TRP and its sister TRPL in fly is still not unequivocal, but it now centers around mechanical effects of PLC-mediated PIP₂ depletion in the membrane and local acidification cause by PIP₂ hydrolysis (Hardie and Franze, 2012; Parnas et al., 2009). In M1-ipRGCs, TRPC6,7 channels probably open also via PIP₂ hydrolysis (Itsuki et al., 2014), but other details differ. In fly, Ca²⁺ influx through the TRP channel greatly amplifies and accelerates photoexcitation (Hardie and Juusola, 2015); in M1-ipRGCs, however, Ca²⁺ appears not to partake in photoexcitation (Graham et al., 2008) albeit possibly in photoadaptation (Do and Yau, 2013). As another variation, melanopsin in microvillous photoreceptors of amphioxus (the most basal chordate) triggers intracellular Ca²⁺ release via the IP₃ receptor (Angueyra et al., 2012; Peinado et al., 2015), similar to that in Limulus ventral photoreceptor (Fein et al., 1984). Thus, mechanistic details in the rhabdomeric motif can be quite diverse. Finally, in the iris-sphincter-muscle controlling pupil size in sub-primate nocturnal and crepuscular mammals (Xue et al., 2011), melanopsin activates PLC-signaling as in M1-ipRGCs (Wang et al., 2017), but causes also an intracellular Ca²⁺ release via an IP₃ receptor—understandably in this case for triggering smooth-muscle contraction—to give a local PLR independent of the canonical PLR via brain circuitry.

For the ciliary motif, two sub-motifs are known, with one involving a decrease, and the other an increase, in intracellular cGMP by light (Yau and Hardie, 2009). For the first, such as in rods and cones and lizard parietal-eye photoreceptor's pinopsin pathway (Su et al., 2006), light activates a phosphodiesterase to lower cGMP, hence closing CNG non-selective cation channels to produce a membrane hyperpolarization. For the second, such as in the scallop hyperpolarizing photoreceptor (Gomez and Nasi, 2000) and a *C. elegans* photoreceptor (Liu et al., 2010), light activates a guanylyl cyclase to elevate cGMP—opening a K⁺-selective channel in scallop (hence hyperpolarization) but a non-selective cation channel in *C. elegans* (hence depolarization). So far, except for jellyfish as an outlier (see below), all established ciliary pathways involve cGMP and not cAMP; correspondingly, CNG channels are more sensitive to cGMP than cAMP.

In ipRGCs, the opening of HCN channels and depolarization by light suggests an increase in cyclic-nucleotide, which we verified experimentally. A key question remains, however. HCN channels are more sensitive to cAMP than cGMP, possibly implicating cAMP being involved. If true, this situation would bear homology to the ciliary photoreceptor in jellyfish, an ancient species in evolution (Koyanagi et al., 2008). There is also some tentative speculation that cAMP precedes cGMP evolutionarily in ciliary phototransduction (Lamb and Hunt, 2017). Unfortunately, our current observations are inconclusive, because the intrinsic light response is blocked by both an adenylyl-cyclase inhibitor and a guanylate-cyclase inhibitor. This cAMP-versus-cGMP question is not easy to settle because the specificities of sensors for them are not all or

none. Ultimately, the answer will require the identities of the G protein and the associated effector enzyme in this pathway.

CNG versus HCN Channels

IpRGCs are the only photoreceptors, vertebrate or invertebrate, known so far to use HCN channels as the effector channel in the ciliary signaling motif of phototransduction. Is there a functional rationale? CNG channels open and close within milliseconds upon binding and unbinding cyclic nucleotide (Biel and Michalakis, 2009; Kaupp and Seifert, 2002). Indeed, the electrical responses of vertebrate rods and cones are dictated in speed more by the upstream transduction biochemistry than by CNG channels' gating kinetics. HCN channels, however, have much slower gating kinetics, whether involving hyperpolarization or cyclic nucleotide (Biel et al., 2009; Seifert et al., 1999; see also Figure 3A). As such, the speed of ipRGCs' electrical response may well be dominated by the channel gating kinetics. This notion is in accord with the much faster intrinsic response upon replacing TRPC6,7 channels with CNGA2 channels (Figure 3C). Although lacking time resolution, the slow HCN-mediated response (even slower than the TRPC6,7-mediated response) may be beneficial for non-image vision, for which the capability of temporal signal integration is probably more important than speed.

Additionally, by being hyperpolarization-activated, HCN channels have an inherent negative-feedback property. Their permeability to both Na^+ and K^+ gives rise to a reversal potential of perhaps -30 mV (Biel et al., 2009), positive enough for triggering action potentials in ipRGCs, but the negative feedback simultaneously limits this depolarization such that the firing is steady and sustained but not intense, avoiding rapid Na-channel inactivation. Such a firing behavior has been reported at least for some ipRGCs (Estevez et al., 2012; Wong, 2012). In mouse M1-ipRGCs, where the HCN current seems to be very small (see Results), the light-initiated firing does appear correspondingly to be more transient, and unable to faithfully signal beyond $\sim 10^9$ photons μm^{-2} s^{-1} (Do and Yau, 2013). It would be useful to examine closely the firing behaviors of M1-, M2-, and M4-ipRGCs and correlate them with their HCN-channel abundance, as well as with their specific functions and connectivities in the brain.

STAR★METHODS

Detailed methods are provided in the online version of this paper and include the following:

- KEY RESOURCES TABLE
- CONTACTS FOR REAGENT AND RESOURCE SHARING
- EXPERIMENTAL MODEL AND SUBJECT DETAILS
 - Animals
 - Cell line
- METHOD DETAILS
 - Patch-clamp recording
 - Light stimulation
 - Drug application
 - Photo-uncaging cAMP or cGMP
 - Immunohistochemistry and other staining procedures

- Virus generation
- Virus injection
- In situ hybridization
- Pupillary light reflex
- Measuring circadian rhythm

● QUANTIFICATION AND STATISTICAL ANALYSIS

SUPPLEMENTAL INFORMATION

Supplemental Information includes six figures and can be found with this article online at <https://doi.org/10.1016/j.cell.2018.08.055>.

ACKNOWLEDGMENTS

We thank L. Cao (Peking University) for rod-suction-pipette recordings to test the drug, ZD7288 and T. Xue (University of Science and Technology China) for initiating some mouse breeding and suggesting the dominant-negative strategy. We thank T.D. Lamb (Australian National University) for discussion on photoreceptor evolution, R. Payne (University of Maryland, College Park) for discussion and unpublished information about the Limulus ventral photoreceptor and Ulrich Müller and Seth Blackshaw for advice on in situ hybridization. We are grateful to the following individuals for providing knockout mouse lines: L. Birnbaumer (NIHES, *Trpc1*^{-/-}, *Trpc3*^{-/-}, *Trpc6*^{-/-}), D.E. Clapham (HHMI Janelia Campus, *Trpc7*^{-/-}), D. Difrancesco (University of Milan, *Hcn4*^{fl/fl}, although eventually not used; see STAR Methods), C. Dulac (Harvard University, *Trpc2*^{-/-}), M. Freichel (University of Saarland, *Trpc4*^{-/-}, *Trpc5*^{-/-}), S. Kuegler (University of Goettingen, AAV6-Epac1-cAMP), S. Siegelbaum (Columbia University, *Hcn1*^{-/-}), A. Ludwig (University of Erlangen, *Hcn2*^{-/-}, *Hcn4*^{fl/fl}), J. Nathans (Johns Hopkins, *rd/rd*), S. Offermanns (Max-Planck Institute, *Gα_q*^{fl/fl}, *Gα₁₁*^{-/-}), R. Reed (Johns Hopkins, main olfactory epithelium cross-sections and CNGA2 cDNA), N. Ryba (NIH/NIDCR, *Plcβ2*^{-/-}), H.-S. Shin (Korea Institute of Science and Technology, *Plcβ1*^{-/-}), M.I. Simon (Caltech, *Gα₁₄*^{-/-}, *Plcβ3*^{-/-}, *Plcβ4*^{-/-}), and T. Wilkie (UT Southwestern Medical Center, *Gα₁₅*^{-/-}). We are also grateful to the following individuals for antibodies: M. Biel (University of Munich, anti-CNGA3, anti-CNGA4, anti-CNGB3), R.S. Molday (University of British Columbia, anti-CNGA1, anti-CNGA2, anti-CNGB1), and F. Müller (Center Advanced European Studies & Research, anti-HCN4, although not providing clear-cut results). We thank T. Shelley for fabricating all custom equipment; L. Ding for mouse-genotyping support; and R. Li, X. Li, and D. Silverman in the Yau lab for comments. Finally, we thank NINDS Multi-photon Imaging Core at JHMI (P30 NS050274) for imaging and data analysis. This work was supported by NIH (EY014596), the António Champalimaud Vision Award, Portugal (to K.-W.Y.), a NARSAD Young Investigator Grant (to Z.J.), and an HHMI International Predoctoral Fellowship (to W.W.S.Y.).

AUTHOR CONTRIBUTIONS

Z.J. did most electrophysiological recordings, all *in situ* hybridization experiments, all whole-animal experiments, and most mouse breedings. W.W.S.Y. did all immunohistochemical and genetic-labeling experiments and made the mut-HCN viral construct. L.C. did some photo-uncaging experiments, did the physiological experiments involving the CNGA2 channel, and made the CNGA2 viral construct. Y.S. did recordings from several *Gα*-KO lines. Z.J. and K.-W.Y. wrote the paper with help from W.W.S.Y., Y.S., and L.C.

DECLARATION OF INTERESTS

The authors declare no competing interests.

Received: October 9, 2017

Revised: March 19, 2018

Accepted: August 21, 2018

Published: September 27, 2018

REFERENCES

- Angueyra, J.M., Pulido, C., Malagón, G., Nasi, E., and Gomez, Mdel.P. (2012). Melanopsin-expressing amphioxus photoreceptors transduce light via a phospholipase C signaling cascade. *PLoS ONE* 7, e29813.
- Applebury, M.L., Antoch, M.P., Baxter, L.C., Chun, L.L., Falk, J.D., Farhangfar, F., Kage, K., Krzystolik, M.G., Lyass, L.A., and Robbins, J.T. (2000). The murine cone photoreceptor: a single cone type expresses both S and M opsins with retinal spatial patterning. *Neuron* 27, 513–523.
- Arendt, D. (2003). Evolution of eyes and photoreceptor cell types. *Int. J. Dev. Biol.* 47, 563–571.
- Arendt, D., Tessmar-Raible, K., Snyman, H., Dorresteijn, A.W., and Wittbrodt, J. (2004). Ciliary photoreceptors with a vertebrate-type opsin in an invertebrate brain. *Science* 306, 869–871.
- Arendt, D., Hausen, H., and Puschke, G. (2009). The “division of labour” model of eye evolution. *Philos. Trans. R. Soc. B Biol. Sci.* 364, 2809–2817.
- Bailes, H.J., and Lucas, R.J. (2013). Human melanopsin forms a pigment maximally sensitive to blue light ($\lambda_{\text{max}} \approx 479$ nm) supporting activation of G(q/11) and G(i/o) signalling cascades. *Proc. Biol. Sci.* 280, 20122987.
- Berson, D.M., Dunn, F.A., and Takao, M. (2002). Phototransduction by retinal ganglion cells that set the circadian clock. *Science* 295, 1070–1073.
- Biel, M., and Michalakis, S. (2009). Cyclic nucleotide-gated channels. *Handb. Exp. Pharmacol.* 191, 111–136.
- Biel, M., Seeliger, M., Pfeifer, A., Kohler, K., Gerstner, A., Ludwig, A., Jaissle, G., Fauser, S., Zrenner, E., and Hofmann, F. (1999). Selective loss of cone function in mice lacking the cyclic nucleotide-gated channel CNG3. *Proc. Natl. Acad. Sci. USA* 96, 7553–7557.
- Biel, M., Wahl-Schott, C., Michalakis, S., and Zong, X. (2009). Hyperpolarization-activated cation channels: from genes to function. *Physiol. Rev.* 89, 847–885.
- Bloomquist, B.T., Shortridge, R.D., Schneuwly, S., Perdew, M., Montell, C., Steller, H., Rubin, G., and Pak, W.L. (1988). Isolation of a putative phospholipase C gene of *Drosophila*, *norpA*, and its role in phototransduction. *Cell* 54, 723–733.
- Chen, L., and Yang, X.L. (2007). Hyperpolarization-activated cation current is involved in modulation of the excitability of rat retinal ganglion cells by dopamine. *Neuroscience* 150, 299–308.
- Chew, K.S., Schmidt, T.M., Rupp, A.C., Kofuji, P., and Trimarchi, J.M. (2014). Loss of *gq/11* genes does not abolish melanopsin phototransduction. *PLoS ONE* 9, e98356.
- Cook, N.J., Molday, L.L., Reid, D., Kaupp, U.B., and Molday, R.S. (1989). The cGMP-gated channel of bovine rod photoreceptors is localized exclusively in the plasma membrane. *J. Biol. Chem.* 264, 6996–6999.
- Dietrich, A., Mederos Y Schnitzler, M., Gollasch, M., Gross, V., Storch, U., Dubrovska, G., Obst, M., Yildirim, E., Salanova, B., Kalwa, H., et al. (2005). Increased vascular smooth muscle contractility in TRPC6-/- mice. *Mol. Cell. Biol.* 25, 6980–6989.
- Dietrich, A., Kalwa, H., Storch, U., Mederos y Schnitzler, M., Salanova, B., Pinkenburg, O., Dubrovska, G., Essin, K., Gollasch, M., Birnbaumer, L., and Gudermann, T. (2007). Pressure-induced and store-operated cation influx in vascular smooth muscle cells is independent of TRPC1. *Pflugers Arch.* 455, 465–477.
- DiFrancesco, D. (1993). Pacemaker mechanisms in cardiac tissue. *Annu. Rev. Physiol.* 55, 455–472.
- Do, M.T.H., and Yau, K.-W. (2010). Intrinsically photosensitive retinal ganglion cells. *Physiol. Rev.* 90, 1547–1581.
- Do, M.T.H., and Yau, K.-W. (2013). Adaptation to steady light by intrinsically photosensitive retinal ganglion cells. *Proc. Natl. Acad. Sci. USA* 110, 7470–7475.
- Do, M.T.H., Kang, S.H., Xue, T., Zhong, H., Liao, H.-W., Bergles, D.E., and Yau, K.-W. (2009). Photon capture and signalling by melanopsin retinal ganglion cells. *Nature* 457, 281–287.
- Ecker, J.L., Dumitrescu, O.N., Wong, K.Y., Alam, N.M., Chen, S.K., LeGates, T., Renna, J.M., Prusky, G.T., Berson, D.M., and Hattar, S. (2010). Melanopsin-expressing retinal ganglion-cell photoreceptors: cellular diversity and role in pattern vision. *Neuron* 67, 49–60.
- Emanuel, A.J., and Do, M.T.H. (2015). Melanopsin tristability for sustained and broadband phototransduction. *Neuron* 85, 1043–1055.
- Emanuel, A.J., Kapur, K., and Do, M.T.H. (2017). Biophysical variation within the M1 Type of ganglion cell photoreceptor. *Cell Rep.* 21, 1048–1062.
- Estevez, M.E., Fogerson, P.M., Ilardi, M.C., Borghuis, B.G., Chan, E., Weng, S., Auferkorte, O.N., Demb, J.B., and Berson, D.M. (2012). Form and function of the M4 cell, an intrinsically photosensitive retinal ganglion cell type contributing to geniculocortical vision. *J. Neurosci.* 32, 13608–13620.
- Fein, A., Payne, R., Corson, D.W., Berridge, M.J., and Irvine, R.F. (1984). Photoreceptor excitation and adaptation by inositol 1,4,5-trisphosphate. *Nature* 311, 157–160.
- Feuda, R., Hamilton, S.C., McInerney, J.O., and Pisani, D. (2012). Metazoan opsin evolution reveals a simple route to animal vision. *Proc. Natl. Acad. Sci. USA* 109, 18868–18872.
- Freichel, M., Suh, S.H., Pfeifer, A., Schweig, U., Trost, C., Weissgerber, P., Biel, M., Philipp, S., Freise, D., Droogmans, G., et al. (2001). Lack of an endothelial store-operated Ca²⁺ current impairs agonist-dependent vasorelaxation in TRP4-/- mice. *Nat. Cell Biol.* 3, 121–127.
- Furuta, Y., Lagutin, O., Hogan, B.L.M., and Oliver, G.C. (2000). Retina- and ventral forebrain-specific Cre recombinase activity in transgenic mice. *Genesis* 26, 130–132.
- Gehring, W.J., and Ikeo, K. (1999). Pax 6: mastering eye morphogenesis and eye evolution. *Trends Genet.* 15, 371–377.
- Givens, R.S., Conrad, P.G., II, Yousef, A.L., and Lee, J.-I. (2003). Photoremoveable protecting groups. In *The CRC Handbook of Organic Photochemistry and Photobiology*, Second Edition, W. Horspool and F. Lenci, eds. (CRC Press), pp. 69.1–69.46.
- Gomez, M.P., and Nasi, E. (2000). Light transduction in invertebrate hyperpolarizing photoreceptors: possible involvement of a Go-regulated guanylate cyclase. *J. Neurosci.* 20, 5254–5263.
- Graham, D.M., Wong, K.Y., Shapiro, P., Frederick, C., Pattabiraman, K., and Berson, D.M. (2008). Melanopsin ganglion cells use a membrane-associated rhabdomeric phototransduction cascade. *J. Neurophysiol.* 99, 2522–2532.
- Hardie, R.C., and Franz, K. (2012). Photomechanical responses in *Drosophila* photoreceptors. *Science* 338, 260–263.
- Hardie, R.C., and Juusola, M. (2015). Phototransduction in *Drosophila*. *Curr. Opin. Neurobiol.* 34, 37–45.
- Hartmann, J., Dragicevic, E., Adelsberger, H., Henning, H.A., Sumser, M., Abramowitz, J., Blum, R., Dietrich, A., Freichel, M., Flockerzi, V., et al. (2008). TRPC3 channels are required for synaptic transmission and motor coordination. *Neuron* 59, 392–398.
- Hatori, M., and Panda, S. (2010). The emerging roles of melanopsin in behavioral adaptation to light. *Trends Mol. Med.* 16, 435–446.
- Hattar, S., Liao, H.W., Takao, M., Berson, D.M., and Yau, K.W. (2002). Melanopsin-containing retinal ganglion cells: architecture, projections, and intrinsic photosensitivity. *Science* 295, 1065–1070.
- Herrmann, S., Stieber, J., Stöckl, G., Hofmann, F., and Ludwig, A. (2007). HCN4 provides a ‘depolarization reserve’ and is not required for heart rate acceleration in mice. *EMBO J.* 26, 4423–4432.
- Hughes, S., Jagannath, A., Hickey, D., Gatti, S., Wood, M., Peirson, S.N., Foster, R.G., and Hankins, M.W. (2015). Using siRNA to define functional interactions between melanopsin and multiple G Protein partners. *Cell. Mol. Life Sci.* 72, 165–179.
- Hughes, S., Jagannath, A., Rodgers, J., Hankins, M.W., Peirson, S.N., and Foster, R.G. (2016). Signalling by melanopsin (OPN4) expressing photosensitive retinal ganglion cells. *Eye (Lond.)* 30, 247–254.

- Itsuki, K., Imai, Y., Hase, H., Okamura, Y., Inoue, R., and Mori, M.X. (2014). PLC-mediated PI(4,5)P₂ hydrolysis regulates activation and inactivation of TRPC6/7 channels. *J. Gen. Physiol.* **143**, 183–201.
- Jiang, H., Lyubarsky, A., Dodd, R., Vardi, N., Pugh, E., Baylor, D., Simon, M.I., and Wu, D. (1996). Phospholipase C beta 4 is involved in modulating the visual response in mice. *Proc. Natl. Acad. Sci. USA* **93**, 14598–14601.
- Jiang, H., Kuang, Y., Wu, Y., Xie, W., Simon, M.I., and Wu, D. (1997). Roles of phospholipase C beta2 in chemoattractant-elicited responses. *Proc. Natl. Acad. Sci. USA* **94**, 7971–7975.
- Kaupp, U.B., and Seifert, R. (2002). Cyclic nucleotide-gated ion channels. *Physiol. Rev.* **82**, 769–824.
- Kim, D., Jun, K.S., Lee, S.B., Kang, N.G., Min, D.S., Kim, Y.H., Ryu, S.H., Suh, P.G., and Shin, H.S. (1997). Phospholipase C isoforms selectively couple to specific neurotransmitter receptors. *Nature* **389**, 290–293.
- Koyanagi, M., Kubokawa, K., Tsukamoto, H., Shichida, Y., and Terakita, A. (2005). Cephalochordate melanopsin: evolutionary linkage between invertebrate visual cells and vertebrate photosensitive retinal ganglion cells. *Curr. Biol.* **15**, 1065–1069.
- Koyanagi, M., Takano, K., Tsukamoto, H., Ohtsu, K., Tokunaga, F., and Terakita, A. (2008). Jellyfish vision starts with cAMP signaling mediated by opsin-G(s) cascade. *Proc. Natl. Acad. Sci. USA* **105**, 15576–15580.
- Lamb, T.D. (2013). Evolution of phototransduction, vertebrate photoreceptors and retina. *Prog. Retin. Eye Res.* **36**, 52–119.
- Lamb, T.D., and Hunt, D.M. (2017). Evolution of the vertebrate phototransduction cascade activation steps. *Dev. Biol.* **431**, 77–92.
- Lamb, T.D., Collin, S.P., and Pugh, E.N., Jr. (2007). Evolution of the vertebrate eye: opsins, photoreceptors, retina and eye cup. *Nat. Rev. Neurosci.* **8**, 960–976.
- Lamb, T.D., Arendt, D., and Collin, S.P. (2009). The evolution of phototransduction and eyes. *Philos. Trans. R. Soc. Lond. B Biol. Sci.* **364**, 2791–2793.
- Lee, S.C., and Ishida, A.T. (2007). Ih without Kir in adult rat retinal ganglion cells. *J. Neurophysiol.* **97**, 3790–3799.
- Li, R.-C., Ben-Chaim, Y., Yau, K.-W., and Lin, C.-C. (2016). Cyclic-nucleotide-gated cation current and Ca²⁺-activated Cl current elicited by odorant in vertebrate olfactory receptor neurons. *Proc. Natl. Acad. Sci. USA* **113**, 11078–11087.
- Liu, J., Ward, A., Gao, J., Dong, Y., Nishio, N., Inada, H., Kang, L., Yu, Y., Ma, D., Xu, T., et al. (2010). C. elegans phototransduction requires a G protein-dependent cGMP pathway and a taste receptor homolog. *Nat. Neurosci.* **13**, 715–722.
- Lucas, R.J. (2013). Mammalian inner retinal photoreception. *Curr. Biol.* **23**, R125–R133.
- Lucas, R.J., Hattar, S., Takao, M., Berson, D.M., Foster, R.G., and Yau, K.-W. (2003). Diminished pupillary light reflex at high irradiances in melanopsin-knockout mice. *Science* **299**, 245–247.
- Ludwig, A., Budde, T., Stieber, J., Moosmang, S., Wahl, C., Holthoff, K., Langebartels, A., Wotjak, C., Munsch, T., Zong, X., et al. (2003). Absence epilepsy and sinus dysrhythmia in mice lacking the pacemaker channel HCN2. *EMBO J.* **22**, 216–224.
- Mataruga, A., Kremmer, E., and Müller, F. (2007). Type 3a and type 3b OFF cone bipolar cells provide for the alternative rod pathway in the mouse retina. *J. Comp. Neurol.* **502**, 1123–1137.
- Meotti, F.C., Lemos de Andrade, E., and Calixto, J.B. (2014). TRP modulation by natural compounds. *Handb. Exp. Pharmacol.* **223**, 1177–1238.
- Michalakis, S., Reisert, J., Geiger, H., Wetzel, C., Zong, X., Bradley, J., Spehr, M., Hüttl, S., Gerstner, A., Pfeifer, A., et al. (2006). Loss of CNGB1 protein leads to olfactory dysfunction and subciliary cyclic nucleotide-gated channel trapping. *J. Biol. Chem.* **281**, 35156–35166.
- Milner, E.S., and Do, M.T.H. (2017). A population representation of absolute light intensity in the mammalian retina. *Cell* **171**, 865–876.
- Nolan, M.F., Malleret, G., Lee, K.H., Gibbs, E., Dudman, J.T., Santoro, B., Yin, D., Thompson, R.F., Siegelbaum, S.A., Kandel, E.R., and Morozov, A. (2003). The hyperpolarization-activated HCN1 channel is important for motor learning and neuronal integration by cerebellar Purkinje cells. *Cell* **115**, 551–564.
- Offermanns, S., Toombs, C.F., Hu, Y.H., and Simon, M.I. (1997). Defective platelet activation in G alpha(q)-deficient mice. *Nature* **389**, 183–186.
- Offermanns, S., Zhao, L.P., Gohla, A., Sarosi, I., Simon, M.I., and Wilkie, T.M. (1998). Embryonic cardiomyocyte hypoplasia and craniofacial defects in G α q/G α 11-mutant mice. *EMBO J.* **17**, 4304–4312.
- Parnas, M., Katz, B., Lev, S., Tzarfaty, V., Dadon, D., Gordon-Shaag, A., Metzner, H., Yaka, R., and Minke, B. (2009). Membrane lipid modulations remove divalent open channel block from TRP-like and NMDA channels. *J. Neurosci.* **29**, 2371–2383.
- Peinado, G., Osorno, T., Gomez, M. del P., and Nasi, E. (2015). Calcium activates the light-dependent conductance in melanopsin-expressing photoreceptors of amphioxus. *Proc. Natl. Acad. Sci. USA* **112**, 7845–7850.
- Pittler, S.J., and Baehr, W. (1991). Identification of a nonsense mutation in the rod photoreceptor cGMP phosphodiesterase beta-subunit gene of the rd mouse. *Proc. Natl. Acad. Sci. USA* **88**, 8322–8326.
- Poetsch, A., Molday, L.L., and Molday, R.S. (2001). The cGMP-gated channel and related glutamic acid-rich proteins interact with peripherin-2 at the rim region of rod photoreceptor disc membranes. *J. Biol. Chem.* **276**, 48009–48016.
- Provencio, I., Jiang, G., De Grip, W.J., Hayes, W.P., and Rollag, M.D. (1998). Melanopsin: An opsin in melanophores, brain, and eye. *Proc. Natl. Acad. Sci. USA* **95**, 340–345.
- Sand, A., Schmidt, T.M., and Kofuji, P. (2012). Diverse types of ganglion cell photoreceptors in the mammalian retina. *Prog. Retin. Eye Res.* **31**, 287–302.
- Schmidt, T.M., and Kofuji, P. (2009). Functional and morphological differences among intrinsically photosensitive retinal ganglion cells. *J. Neurosci.* **29**, 476–482.
- Schmidt, T.M., Chen, S.K., and Hattar, S. (2011). Intrinsically photosensitive retinal ganglion cells: many subtypes, diverse functions. *Trends Neurosci.* **34**, 572–580.
- Seifert, R., Scholten, A., Gauss, R., Mincheva, A., Lichter, P., and Kaupp, U.B. (1999). Molecular characterization of a slowly gating human hyperpolarization-activated channel predominantly expressed in thalamus, heart, and testis. *Proc. Natl. Acad. Sci. USA* **96**, 9391–9396.
- Shichida, Y., and Matsuyama, T. (2009). Evolution of opsins and phototransduction. *Philos. Trans. R. Soc. B Biol. Sci.* **364**, 2881–2895.
- Stieber, J., Herrmann, S., Feil, S., Löster, J., Feil, R., Biel, M., Hofmann, F., and Ludwig, A. (2003). The hyperpolarization-activated channel HCN4 is required for the generation of pacemaker action potentials in the embryonic heart. *Proc. Natl. Acad. Sci. USA* **100**, 15235–15240.
- Stowers, L., Holy, T.E., Meister, M., Dulac, C., and Koentges, G. (2002). Loss of sex discrimination and male-male aggression in mice deficient for TRP2. *Science* **295**, 1493–1500.
- Su, C.-Y., Luo, D.-G., Terakita, A., Shichida, Y., Liao, H.-W., Kazmi, M.A., Sakmar, T.P., and Yau, K.-W. (2006). Parietal-eye phototransduction components and their potential evolutionary implications. *Science* **311**, 1617–1621.
- Van Hook, M.J., and Berson, D.M. (2010). Hyperpolarization-activated current (I(h)) in ganglion-cell photoreceptors. *PLoS ONE* **5**, e15344.
- Venkatachalam, K., and Montell, C. (2007). TRP channels. *Annu. Rev. Biochem.* **76**, 387–417.
- Vöcking, O., Kourtesis, I., Tumu, S.C., and Hausen, H. (2017). Co-expression of xenopsin and rhabdomeric opsin in photoreceptors bearing microvilli and cilia. *eLife* **6**, e23435.
- Vopalensky, P., Pergner, J., Liegertova, M., Benito-Gutierrez, E., Arendt, D., and Kozmík, Z. (2012). Molecular analysis of the amphioxus frontal eye unravels the evolutionary origin of the retina and pigment cells of the vertebrate eye. *Proc. Natl. Acad. Sci. USA* **109**, 15383–15388.

- Wang, Q., Yue, W.W.S., Jiang, Z., Xue, T., Kang, S.H., Bergles, D.E., Mikoshiba, K., Offermanns, S., and Yau, K.W. (2017). Synergistic signaling by light and acetylcholine in mouse iris sphincter muscle. *Curr. Biol.* 27, 1791–1800.
- Warren, E.J., Allen, C.N., Brown, R.L., and Robinson, D.W. (2006). The light-activated signaling pathway in SCN-projecting rat retinal ganglion cells. *Eur. J. Neurosci.* 23, 2477–2487.
- Wettschureck, N., Rütten, H., Zywiertz, A., Gehring, D., Wilkie, T.M., Chen, J., Chien, K.R., and Offermanns, S. (2001). Absence of pressure overload induced myocardial hypertrophy after conditional inactivation of Galphaq/Galpha11 in cardiomyocytes. *Nat. Med.* 7, 1236–1240.
- Wong, K.Y. (2012). A retinal ganglion cell that can signal irradiance continuously for 10 hours. *J. Neurosci.* 32, 11478–11485.
- Xie, W., Samoriski, G.M., McLaughlin, J.P., Romoser, V.A., Smrcka, A., Hinkle, P.M., Bidlack, J.M., Gross, R.A., Jiang, H., and Wu, D. (1999). Genetic alteration of phospholipase C beta3 expression modulates behavioral and cellular responses to mu opioids. *Proc. Natl. Acad. Sci. USA* 96, 10385–10390.
- Xu, X., Croy, J.T., Zeng, W., Zhao, L., Davignon, I., Popov, S., Yu, K., Jiang, H., Offermanns, S., Muallem, S., and Wilkie, T.M. (1998). Promiscuous coupling of receptors to Gq class α subunits and effector proteins in pancreatic and submandibular gland cells. *J. Biol. Chem.* 273, 27275–27279.
- Xue, T., Marbán, E., and Li, R.A. (2002). Dominant-negative suppression of HCN1- and HCN2-encoded pacemaker currents by an engineered HCN1 construct: insights into structure-function relationships and multimerization. *Circ. Res.* 90, 1267–1273.
- Xue, T., Do, M.T., Riccio, A., Jiang, Z., Hsieh, J., Wang, H.C., Merbs, S.L., Welsbie, D.S., Yoshioka, T., Weissgerber, P., et al. (2011). Melanopsin signaling in mammalian iris and retina. *Nature* 479, 67–73.
- Yau, K.W., and Hardie, R.C. (2009). Phototransduction motifs and variations. *Cell* 139, 246–264.

STAR★METHODS

KEY RESOURCES TABLE

REAGENT or RESOURCE	SOURCE	IDENTIFIER
Antibodies		
Mouse monoclonal anti-bovine CNGA1	Cook et al., 1989	Cat#PMc1D1
Mouse monoclonal anti-mouse CNGA2	Li et al., 2016	N/A
Rabbit polyclonal anti-mouse CNGA3	Biel et al., 1999	N/A
Guinea pig polyclonal anti-mouse CNGA4	Michalakis et al., 2006	N/A
Mouse monoclonal anti-human CNGB1	Poetsch et al., 2001	Cat#GARP4B1
Rabbit polyclonal anti-mouse CNGB3	Michalakis et al., 2006	N/A
Rabbit polyclonal anti-GFP	Invitrogen	Cat#A11122
Chicken polyclonal anti-β-galactosidase	Abcam	Cat#Ab9361
Mouse monoclonal anti-V5-tag	Thermo Fisher Scientific	Cat#R960-25
Alexa Fluor 488 goat anti-mouse IgG	Thermo Fisher Scientific	Cat#A11029
Alexa Fluor 488 goat anti-rabbit IgG	Thermo Fisher Scientific	Cat#A11034
Alexa Fluor 488 goat anti-guinea pig IgG	Thermo Fisher Scientific	Cat#A11073
Alexa Fluor 568 goat anti-mouse IgG	Thermo Fisher Scientific	Cat#A11031
Alexa Fluor 647 goat anti-chicken IgG	Thermo Fisher Scientific	Cat#A11039
Experimental Models: Organisms/Strains		
C57BL/6J	Jackson Laboratory	Cat#000664
BAC transgenic <i>Opn4:tdTomato</i>	Do et al., 2009	N/A
<i>Opn4-Cre</i>	Wang et al., 2017	N/A
<i>Opn4-Cre;Rosa-tdTomato</i> (Ai9)	Wang et al., 2017	N/A
<i>Opn4</i> ^{-/-}	Lucas et al., 2003	N/A
<i>rd/rd</i>	Pittler and Baehr, 1991	N/A
<i>Six3-cre</i>	Furuta et al., 2000	N/A
<i>Trpc1</i> ^{-/-}	Dietrich et al., 2007	N/A
<i>Trpc2</i> ^{-/-}	Stowers et al., 2002	N/A
<i>Trpc3</i> ^{-/-}	Hartmann et al., 2008	N/A
<i>Trpc4</i> ^{-/-}	Freichel et al., 2001	N/A
<i>Trpc5</i> ^{-/-}	Xue et al., 2011	N/A
<i>Trpc6</i> ^{-/-}	Dietrich et al., 2005	N/A
<i>Trpc7</i> ^{-/-}	Xue et al., 2011	N/A
<i>Gα_q</i> ^{fl/fl}	Wettschureck et al., 2001	N/A
<i>Gα₁₁</i> ^{-/-}	Offermans et al., 1998	N/A
<i>Gα₁₄</i> ^{-/-}	Xu et al., 1998	N/A
<i>Gα₁₅</i> ^{-/-}	Xu et al., 1998	N/A
<i>Plcβ1</i> ^{-/-}	Kim et al., 1997	N/A
<i>Plcβ2</i> ^{-/-}	Jiang et al., 1997	N/A
<i>Plcβ3</i> ^{-/-}	Xie et al., 1999	N/A
<i>Plcβ4</i> ^{-/-}	Jiang et al., 1996	N/A
<i>HCN4nLacZ/H2BGFP</i>	Jackson Laboratory	Cat#024284
<i>Hcn1</i> ^{-/-}	Nolan et al., 2003	N/A
<i>Hcn2</i> ^{-/-}	Ludwig et al., 2003	N/A
<i>Hcn4</i> ^{fl/fl}	Stieber et al., 2003	N/A
Chemicals, Peptides, and Recombinant Proteins		
Ames' medium	Sigma	Cat#A1420
DL-2-Amino-4-phosphonobutyric acid	Sigma	Cat#A1910

(Continued on next page)

Continued

REAGENT or RESOURCE	SOURCE	IDENTIFIER
DNQX	Sigma	Cat#D0540
DL-2-Amino-5-phosphonopentanoic acid	Sigma	Cat#A5282
Hexamethonium	Sigma	Cat#H0879
Picrotoxin	Sigma	Cat#P1675
Strychnine	Sigma	Cat#S0532
Ruthenium Red	Sigma	Cat#R-2751
ZD7288	Sigma	Cat#Z3777
Forskolin	Millipore Corp	Cat#344270
IBMX	Thermo Fisher Scientific	Cat#PHZ1124
LY83583	Cayman Chemical	Cat#70230
ST034307	Tocris	Cat#6271
BCMCM-cAMP	Biolog	Cat#B016
BCMCM-cGMP	Biolog	Cat#B017
Newborn calf serum	Sigma	Cat#12023C
Normal goat serum	Sigma	Cat#S26
Rhodamine-conjugated peanut agglutinin	Vector Laboratories	Cat#RL-1072
Anti-fade mounting medium with DAPI	Vector Laboratories	Cat#H-1200
Dulbecco's Modified Eagle Medium	Thermo Fisher Scientific	Cat#11965
Opti-MEM I Reduced-Serum Medium	Thermo Fisher Scientific	Cat#31985-070
TransIT-293	Mirus Bio	Cat#MIR 2705
X-gal	Sigma	Cat#10651745001
RNAscope Multiplex Fluorescent Reagent Kit v2	Advanced Cell Diagnostics	Cat#323110
RNAscope Probe-Mm-Hcn4	Advanced Cell Diagnostics	Cat#4211271
RNAscope Probe-Mm-Opn4-C2	Advanced Cell Diagnostics	Cat#438061-C2
RNAscope 3-plex Negative Control Probe	Advanced Cell Diagnostics	Cat#320871
TSA Plus Cyanine 5	PerkinElmer	Cat#NEL745E001KT
TSA Plus fluorescein	PerkinElmer	Cat#NEL741E001KT
Bacterial and Virus Strains		
AAV2-CMV-CRE-GFP	UNC Vector Core	AAV2-CMV-CRE-GFP
AAV2-CMV-GFP	UNC Vector Core	AAV2-CRE-GFP
Experimental Models: Cell Lines		
HEK293	American Type Culture Collection	Cat#CRL-1573
Recombinant DNA		
pAAV.CMV.PI.EGFP.WPRE.bGH	Penn Vector Core	Cat#p0101
Hcn2 cDNA in pENTR223.1	Dharmacon	Cat#OMM5896-202525167
pEZYmyc-his plasmid	Addgene	#18701
gBlock fragment for adding V5 tag	IDT	N/A
gBlock fragment for inserting AAA mutation	IDT	N/A
Cnga2 cDNA	Gift from Dr. Randall Reed	N/A
Software and Algorithms		
Igor Pro 6.3.7.2	WaveMetrics	N/A
ClockLab 3	ActiMetrics	N/A

CONTACTS FOR REAGENT AND RESOURCE SHARING

Further information and requests for resources and reagents should be directed to and will be fulfilled by the Lead Contact, King-Wai Yau (kwyau@jhmi.edu).

EXPERIMENTAL MODEL AND SUBJECT DETAILS

Animals

The experimental procedures on animals followed the guidelines of the Animal Care and Use committee of the Johns Hopkins University School of Medicine. The mouse lines in the [Key Resources Table](#) and their crossings have been used in this study. Because it is not feasible to have WT littermate controls for complex genotypes, we used as controls mice of the C57BL/6J strain, which is the genetic background for many of the lines. Both male and female mice were used in all experiments. Because constitutive $G\alpha_q^{-/-}$ has a very high mortality rate before birth ([Offermanns et al., 1997](#)), we crossed an *Opn4-Cre* line with $G\alpha_q^{fl/fl}$ line to achieve conditional deletion of G_q specifically in ipRGCs. We also generated successfully *Opn4-Cre;G\alpha_q^{fl/fl};G\alpha_{11}^{-/-};G\alpha_{14}^{-/-}* mice, despite $G\alpha_q$ and $G\alpha_{14}$ being linked genes with a low recombination probability of only ~3 in 1000. Likewise, $Hcn4^{-/-}$ is embryonic lethal ([Stieber et al., 2003](#)), entailing the use of $Hcn4^{fl/fl}$.

Cell line

HEK293 cells were retrieved from a trusted source (American Type Culture Collection) and were not authenticated after purchase. All cells were cultured at 37°C, with 95% air and 5% CO₂. Cells were cultured to ~80% confluence on round coverslips (8-mm diameter, #1 thickness) in Dulbecco's Modified Eagle Medium (DMEM, Thermo Fisher Scientific) in a 6-well plate. *Hcn4* cDNA was cloned into a pCIG-DV vector containing also a nuclear GFP cDNA sequence under a separate promoter. Plasmid DNA (~1 µg/µl) for this pCIG-Hcn4-nGFP construct was purified, and mixed with Opti-MEM I Reduced-Serum Medium (Thermo Fisher Scientific) and a transfection reagent (TransIT-293, Mirus Bio) at conditions suggested in the product manual. Where applicable, purified AAV-mut-HCN2 (see [Figure 5A](#)) plasmid DNA was also included in the above mixture. After 30 min of incubation, the mixture was added dropwise onto the cultured cells. Cells were allowed to incubate in DMEM for 48 – 72 hours before being used for electrophysiological experiments.

METHOD DETAILS

Patch-clamp recording

Mice were dark-adapted for more than 3 hours before experiment. After euthanasia, retina was dissected from the eye under infrared light. Isolated retinas were cut into 4 pieces and stored in Ames' medium (Sigma) bubbled with 95% O₂/5% CO₂ at room temperature in darkness until use. When used, a retinal piece was held in the recording chamber with ganglion-cell side up by a U-shaped platinum frame strung with nylon fiber. During recording, retina was perfused with Ames' medium bubbled with 95% O₂/5% CO₂. Synaptic transmission was blocked by 250-µM DL-2-Amino-4-phosphonobutyric acid (Sigma), 20-µM DNQX (Sigma), 50-µM DL-2-Amino-5-phosphonopentanoic acid (Sigma), 100-µM Hexamethonium (Sigma), 100-µM Picrotoxin (Sigma), and 1-µM Strychnine (Sigma). All of the synaptic blockers were directly dissolved in Ames' medium, except Strychnine (dissolved in DMSO to prepare a 10-mM stock solution).

Patch electrodes (5–7 MΩ) were pulled from borosilicate capillaries (GC150-10, Harvard Apparatus) and filled with internal solution containing typically (in mM): 120 K-gluconate, 5 NaCl, 4 KCl, 10 HEPES, 2 EGTA, 4 ATP-Mg, 0.3 GTP-Na₂ and 7 Phosphocreatine-Tris, with pH adjusted to 7.3 with KOH. Live ipRGCs were genetically labeled by the *tdTomato* transgene in the BAC transgenic *Opn4:tdTomato* line for all recordings except for the *Opn4-Cre;G\alpha_q^{fl/fl};G\alpha_{11}^{-/-};G\alpha_{14}^{-/-}* and *Opn4-Cre;Hcn4^{fl/fl}* genotype, in which ipRGCs were labeled by Cre-driven *Rosa-tdTomato* (Ai9) reporter to further verify Cre-recombinase expression. Fluorescent signal was imaged by a Nikon CCD camera with data acquisition synchronized with a 20-ms flash of epi-fluorescence excitation light. The total exposure time to excitation light before recording was < 500 ms. We observed a more complex M2-response, with fast and slow components, than has been described previously ([Ecker et al., 2010](#); [Schmidt and Kofuji, 2009](#)), probably because the cells studied by us were more dark-adapted owing to the brief excitation light.

Whole-cell patch-clamp recording was made at 30–32°C with an Axon Instruments Multiclamp 700B amplifier. Series resistance of patch electrodes was 10–30 MΩ. Liquid-junction potential (measured to be –13 mV) has been corrected. Cells were voltage-clamped at –66 mV unless indicated otherwise in some experiments. All photocurrent amplitudes were measured on traces low-pass filtered at 20 Hz (8-pole Bessel). However, for clearer visualization, all representative light responses shown were low-pass filtered at 2 Hz (8-pole Bessel), except for the M1-response in [Figures 1A, 2B, and S2](#), as well as CNGA2-mediated current in [Figure 3C](#), which were low-pass filtered at 20 Hz (8-pole Bessel) in order to capture the fast response of M1-ipRGCs or CNGA2-mediated current. Recordings of I_h tail current were low-pass filtered at 100 Hz (8-pole Bessel filter). M1-, M2-, and M4-ipRGCs were initially targeted based on *tdTomato*-fluorescence intensity and soma size. Alexa Fluor 568 hydrazide (20 µM) was dialyzed through the whole-cell recording pipette to reveal the cell's dendritic morphology. The subtype identities of the recorded cells were further validated by post-recording morphological analysis of dendritic arbors.

Light stimulation

A 75-W Xe-arc lamp was used for eliciting light response from ipRGCs. A water filter was inserted into the light path to reduce infrared light. Full-field, unattenuated white light (200-ms, at an intensity equivalent to 1.75×10^{10} photons $\mu\text{m}^{-2} \text{ sec}^{-1}$ of 480-nm light for melanopsin, with the conversion achieved by response-matching in the linear range) was used for all patch-clamp recording

experiments. For pupillary light reflex, a LED light (λ_{max} at 505 nm, 30-nm bandwidth) provided the light stimulation, as described previously (Xue et al., 2011). Light intensities were routinely calibrated with a radiometer.

Drug application

Blockers for ion channels or effector enzymes were applied in bath solution together with synaptic blockers mentioned above. Ruthenium Red (20 μM , Sigma) and LY83583 (120 μM , Cayman Chemical) were directly dissolved in the bath solution. ST034307 (50 μM , Tocris) was diluted from a 100-mM stock solution in DMSO. ZD7288 (50 μM , Sigma) was diluted from a 100-mM stock solution in distilled water.

Forskolin (40 μM , Millipore) and IBMX (1 mM, Thermo Fisher Scientific) dissolved in bath solution were locally applied using a Picospritzer II connected to a glass pipette with 1-2 μm tip diameter. The puffing pipette was placed within 60 μm of the cell soma. The Picospritzer was operated at a pressure of 1-2 psi. Forskolin (100-mM DMSO stock solution) and IBMX were dissolved in external solution with synaptic blockers.

Photo-uncaging cAMP or cGMP

Caged-compound (50- μM BCMCM-cAMP or BCMCM-cGMP) was included in the whole-cell recording pipette. Recordings were made from *Opn4*^{-/-} ipRGCs in order to eliminate the intrinsic light response originating from melanopsin. Another white light beam (0.12 $\mu\text{W} \mu\text{m}^{-2}$) from a Hg-lamp was used to achieve higher light intensity than that for eliciting the intrinsic light response (see above), particularly in the UV portion, in order to give more effective photo-uncaging (excitation $\lambda_{\text{max}} = 347$ nm). A small light spot (40- μm in diameter) was used to minimize photo-uncaging in the recording pipette. The first uncaging-flash was applied at 5 min after achieving whole-cell recording mode, in order to allow sufficient dialysis of caged-compound. The interval between uncaging flashes was 5 min. Control experiments on M4-cells were done under identical conditions but with no caged-compound loaded; as expected, no photocurrent was elicited (not shown).

Immunohistochemistry and other staining procedures

For flat-mount mouse retinas, animals were typically subject to transcardiac perfusion with phosphate-buffered saline (PBS) followed by 4% paraformaldehyde (PFA). Retinas were dissected and post-fixed with 4% PFA at room temperature for 30 minutes, then washed with PBS containing 0.5% Triton X-100 (PBST). To block non-specific antibody binding, retinas were incubated overnight at 4°C with blocking solution – 10% newborn calf serum (Sigma-Aldrich), 10% normal goat serum (Sigma-Aldrich) or 10 mg/ml tyramide blocking reagent (Thermo Fisher Scientific). Primary-antibody incubation was done in the same blocking solution at 4°C for 3-5 days. After several rinses, retinas were incubated with the appropriate fluorophore-conjugated secondary antibodies (Thermo Fisher Scientific) at 1:500 dilution in blocking solution in the dark for 3 hours at room temperature or overnight at 4°C. Rhodamine-conjugated peanut agglutinin (PNA, Vector Laboratories) was included in this step at 1:1000 dilution in cases where cones were to be labeled (Figure 3B). Lastly, retinas were washed, mounted with the above DAPI-containing anti-fade medium (Vector Laboratories), and coverslipped.

For cryosections, an eyeball was isolated from a perfused animal and post-fixed with 4% PFA for 30 min at 4°C. The anterior chamber and the lens were removed and the remaining eyecup was post-fixed for additionally 3 hr at 4°C. The eyecup was then washed with PBS and equilibrated in 30% sucrose at 4°C for at least one day. Finally, the eyecup was cryopreserved in Optimal Cutting Temperature (OCT) compound (Tissue-Tek) and sectioned at a thickness of 14 μm . Coronal cryosections of olfactory tissues were gifts from Dr. Randall Reed (Johns Hopkins). All cryosections were stored at -80°C until use. Immunohistochemistry on cryosections followed the same procedure as above except that the primary-antibody incubation was performed at 4°C overnight whereas the blocking step and the secondary-antibody incubation were both done at room temperature for 1 hr.

Primary antibodies used in this work include (dilutions and sources in brackets): a mouse anti-bovine CNGA1 monoclonal antibody (Cook et al., 1989) (1:20 for flat-mount retina, 1:10 for retinal section, gift from Dr. Robert Molday, Figure 3B), a mouse anti-mouse CNGA2 mouse monoclonal antibody against mouse protein (1:10 for flat-mount retina, 1:20 for olfactory section, gift from Dr. Robert Molday, Figure 3B), a rabbit anti-mouse CNGA3 polyclonal antibody (Biel et al., 1999) (1:2000, gift from Dr. Martin Biel, Figure 3B), a guinea pig anti-mouse CNGA4 polyclonal antibody (Michalakis et al., 2006) (1:20 for flat-mount retina, 1:250 for olfactory section, gift from Dr. Martin Biel, Figure 3B), a mouse anti-human CNGB1 monoclonal antibody (Poetsch et al., 2001) (1:20 for flat-mount retina, 1:10 for retinal section, gift from Dr. Robert Molday, Figure 3B), a rabbit anti-mouse CNGB3 polyclonal antibody (Michalakis et al., 2006) (1:2000, gift from Dr. Martin Biel, Figure 3B), a rabbit anti-GFP polyclonal antibody (1:500, from Invitrogen, Figures 5B, 5C, and 5E), a chicken anti- β -galactosidase polyclonal antibody (1:1000, Ab9361 from Abcam, Figure 5E), and a mouse anti-V5-tag monoclonal antibody (1:1000, from Thermo Fisher #R960-25, Figures 5B and 5C).

For X-gal staining (Figure S6), retinas were dissected from *HCN4nLacZ/H2BGFP* mice perfused transcardially with PBS and freshly-made X-gal fixative (0.2% glutaraldehyde and 2 mM MgCl₂ in PBS). After post-fixation with X-gal fixative at room temperature for 30 minutes, the retinas were rinsed with detergent buffer (2 mM MgCl₂, 0.01% Na-deoxycholate, and 0.02% Nonidet P-40 in PBS). Staining was done by incubating the retinas in detergent buffer containing 5 mM potassium ferricyanide, 5 mM potassium ferrocyanide, and 1 mg/ml X-gal until signals reached good intensities.

Virus generation

For constructing a viral vector to drive expression of a dominant-negative HCN2, we used the pAAV.CMV.PI.EGFP.WPRE.bGH (p0101) plasmid from the Penn Vector Core (University of Pennsylvania) as the backbone vector. The WT mouse HCN2 cDNA sequence was transferred from a pENTR223.1 (OMM5896-202525167, Dharmacon) vector to p0101 by Gateway cloning first into pEZYmyc-his plasmid (#18701, Addgene) and subsequent restriction cloning (by NotI and HindIII enzymes). To add a V5 tag to the C-terminal of HCN2 for identifying infected cells, a gBlock fragment carrying an in-frame V5 insertion was synthesized and was used to replace the corresponding sequence in p0101 by restriction cloning (at BspEI and HindIII sites). To introduce the dominant-negative mutation (replacement of the G₄₀₂Y₄₀₃G₄₀₄ motif in the pore region by three alanines), the corresponding sequence in p0101 was again replaced by a gBlock fragment carrying the mutation by restriction cloning (at SacI and Acc65I sites). The final plasmid (Figure 5A) was sequenced and sent to Penn Vector Core for production of viral particles (final yield of $8.82 \times 10^{11} \mu\text{l}^{-1}$).

For constructing a viral vector to express CNGA2, we also used p0101 plasmid as the backbone vector. The WT rat CNGA2 cDNA sequence (kindly offered by Dr. Randall Reed) was inserted into the p0101 vector by restriction cloning (at EagI and BamHI sites). A V5 tag was added to the C-terminal of CNGA2 by PCR method. The CNGA2-V5 plasmid was also sent to Penn Vector Core for production of viral particles (final yield of $4.08 \times 10^{13} \mu\text{l}^{-1}$).

AAV2-CMV-CRE-GFP and AAV2-CMV-GFP viruses were purchased from the vector core at the University of North Carolina.

Virus injection

For identifying the G-protein isoforms involved in ipRGCs' phototransduction, AAV2-CMV-Cre-GFP virus ($5.4 \times 10^{12} \mu\text{l}^{-1}$, 3 μL per eye) was injected into the vitreous of the eyes of $G\alpha_q^{/\text{ff}};G\alpha_{11}^{-/-};G\alpha_{14}^{-/-};Opn4:tdTomato$ mice. After at least 2 weeks, infected ipRGCs were identified by GFP and tdTomato signals.

To test the involvement of HCN channels in the phototransduction pathway of ipRGCs, we performed intra-vitreal injection of a mixture (3 μL per eye) of AAV2-mut-HCN2 and AAV-CMV-GFP viruses at a 1:1 volume ratio (virus concentration $8.82 \times 10^{11} \mu\text{l}^{-1}$ and $1.22 \times 10^{12} \mu\text{l}^{-1}$, respectively) into *Trpc6,7^{-/-}* mice, and achieved about 80% co-infection rate after 2 weeks (Figure 5C), indicating sufficient infection-overlap for letting GFP-fluorescence guide the search of mut-HCN2-expressing cells for recording. We aimed at retinal ganglion cells having both GFP (suggestive of co-infection by AAV2-mut-HCN2) and tdTomato signals (indicative of melanopsin expression), and further confirmed the infection by a significant reduction of the I_h current (more than 2/3 reduction of WT I_h current: M2, $I_h < 5\text{pA}$; M4, $I_h < 15 \text{ pA}$).

To detect the production of cyclic nucleotides in phototransduction pathway, we performed intra-vitreal injection of a mixture (3 μL per eye) of AAV2-CNGA2-V5 and AAV-CMV-GFP viruses at a 1:1 volume ratio (virus concentration $4.08 \times 10^{13} \mu\text{l}^{-1}$ and $1.22 \times 10^{12} \mu\text{l}^{-1}$, respectively) into *Trpc6,7^{-/-}* mice. To target for ipRGCs that expressed CNGA2, we recorded retinal ganglion cells showing both GFP and tdTomato signals.

In situ hybridization

RNA *in situ* hybridization was performed with RNAscope Multiplex Fluorescent Reagent Kit v2 (ACD, Advanced Cell Diagnostics, #323110) following the manufacturer's protocol. Fresh eyecups, without prior fixation, were embedded into OCT compound (Tissue-Tek) and immediately frozen by liquid nitrogen. The frozen blocks were sectioned at a thickness of 16 μm . Catalog probes (#421271 and #438061-C2) targeting *Hcn4* or *Opn4* mRNA and the negative control probe (#320871) targeting *dapB* mRNA were purchased from ACD. TSA Plus Cyanine 5 (#NEL745E001KT) and TSA Plus fluorescein (#NEL741E001KT) were used for developing HRP-C1 and HRP-C2 signals, respectively. The fluorescent signal was visualized and captured by a Zeiss LSM 880 confocal microscope.

Pupillary light reflex

The mice were kept in 12/12-hr light/dark (L/D) cycle. All PLR experiments were performed on hand-held, awake mice under light-adapted conditions, in the time window of 3 hr after light-on and 1 hr before light-off. Consensual PLR was recorded by an infrared camera under infrared LED illumination (wavelength > 850 nm) and measured at peak during 1-min step-light stimulation and normalized to pupil area in dark condition. Video of the contralateral eye was recorded and digitalized at a frame rate of 5 Hz. A data-acquisition board (NI USB-6211, National Instruments) and LabView software were used to synchronize the light stimulation and data acquisition. The pupil area was measured using the oval selection and measure tools. Light stimulation was provided on the contralateral eye with a 505-nm LED light (Xue et al., 2011). Animals were light-adapted with 1000-lux white light for more than 3 hours before experiment. Under dark-adapted conditions, the *Trpc6,7^{-/-};rd/rd* genotype had no consensual PLR. PLR is expressed as MFC (Maximum Fractional Constriction), where MFC = 1 - Normalized Pupil Area in Light = 1 - (Pupil Area in Light/Pupil Area in Darkness).

Measuring circadian rhythm

Wheel-running experiments were performed on 4- to 12-month-old mice, which were individually kept in cages with a wheel. The wheel rotation was constantly monitored by CLOCKLAB SUITE Circadian Mouse System. 1000-lux light from a white fluorescent light bulb was applied in the light period. In the dark period, an infrared light bulb was turned on to maintain constant temperature in the chamber. Data were analyzed by CLOCKLAB 3 software. The onset of the activity and the period of circadian cycle were determined

by the software's built-in algorithm. Phase-shift rate was calculated using linear regression fit. The mice were kept first in 12/12 hr L/D cycle for 6 days. Afterward, a 6-hr phase advance was imposed, followed by a 6-hr backward phase-shift. At the end, the mice were kept in constant darkness for at least 6 days to measure circadian periods.

QUANTIFICATION AND STATISTICAL ANALYSIS

Statistical analysis was performed in Microsoft Excel. Data are all expressed as mean \pm SEM. Unpaired two-tailed Student's test was used to determine statistical significance. The "n" numbers for each experiment are provided in the text and figure legends. For immunocytochemistry and *in situ* hybridization results, experiments were repeated on at least 2 animals.

Supplemental Figures

Cell

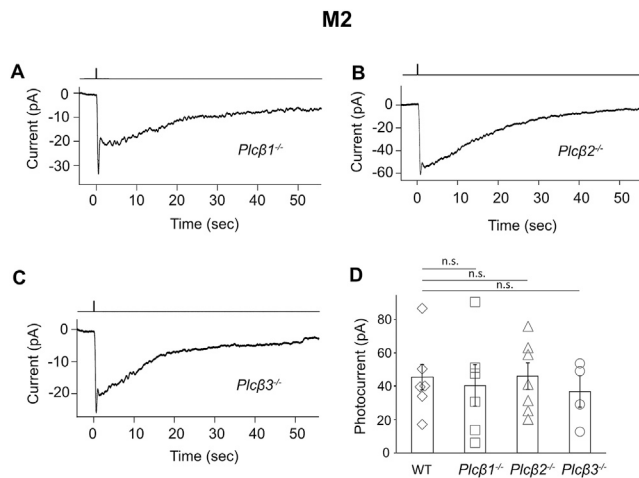


Figure S1. M2-ipRGCs with *Plcβ1*^{-/-}, *Plcβ2*^{-/-}, or *Plcβ3*^{-/-} Genotype Have Normal Light Responses, Related to Figure 2

(A–C) Intrinsic responses with both fast and slow components, similar to WT (Figure 1A middle).

(D) Collective data of peak photocurrents (mean \pm SEM, $n = 6, 6, 7, 4$ cells from at least 2 animals in each group). n.s. indicates being not statistically significant, $p > 0.05$. WT data are reproduced from Figure 1E.

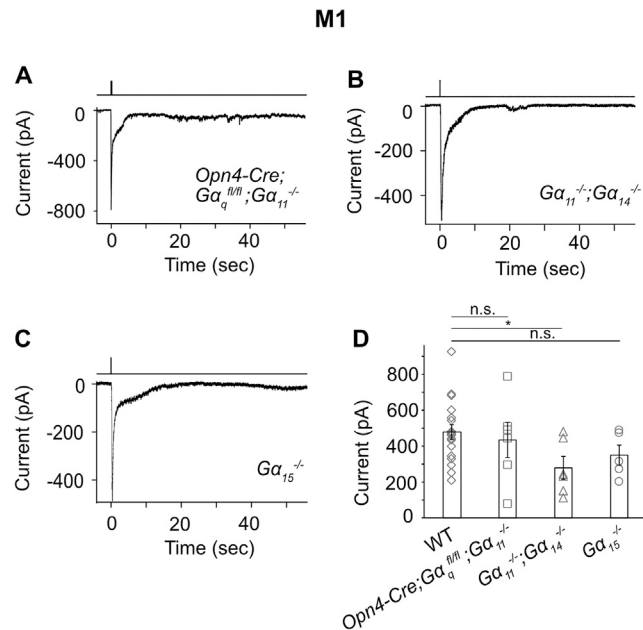


Figure S2. Intrinsic Light Response of M1-ipRGCs in Different G Protein Knockouts, Related to Figure 2

(A–D) (A) $\text{Open4-Cre}; \text{G}\alpha_q^{+/+}; \text{G}\alpha_{11}^{-/-}$, (B) $\text{G}\alpha_{11}^{-/-}; \text{G}\alpha_{14}^{-/-}$, (C) $\text{G}\alpha_{15}^{-/-}$ genotypes and (D) Collective data of saturated photocurrents (mean \pm SEM; n = 18, 6, 6 and 5 cells from at least 2 animals in each group). * indicates $p < 0.05$; n.s. indicates no significant difference, with $p > 0.05$. The data suggest that, possibly, deleting $\text{G}\alpha_{11}^{-/-}; \text{G}\alpha_{14}^{-/-}$ and leaving only $\text{G}\alpha_q$ in place does not lead to a fully intact response. Hence, the functional redundancy among $\text{G}\alpha_{11}$, $\text{G}\alpha_{14}$ and $\text{G}\alpha_q$ in M1-phototransduction is probably incomplete. We have not examined this point further, however.

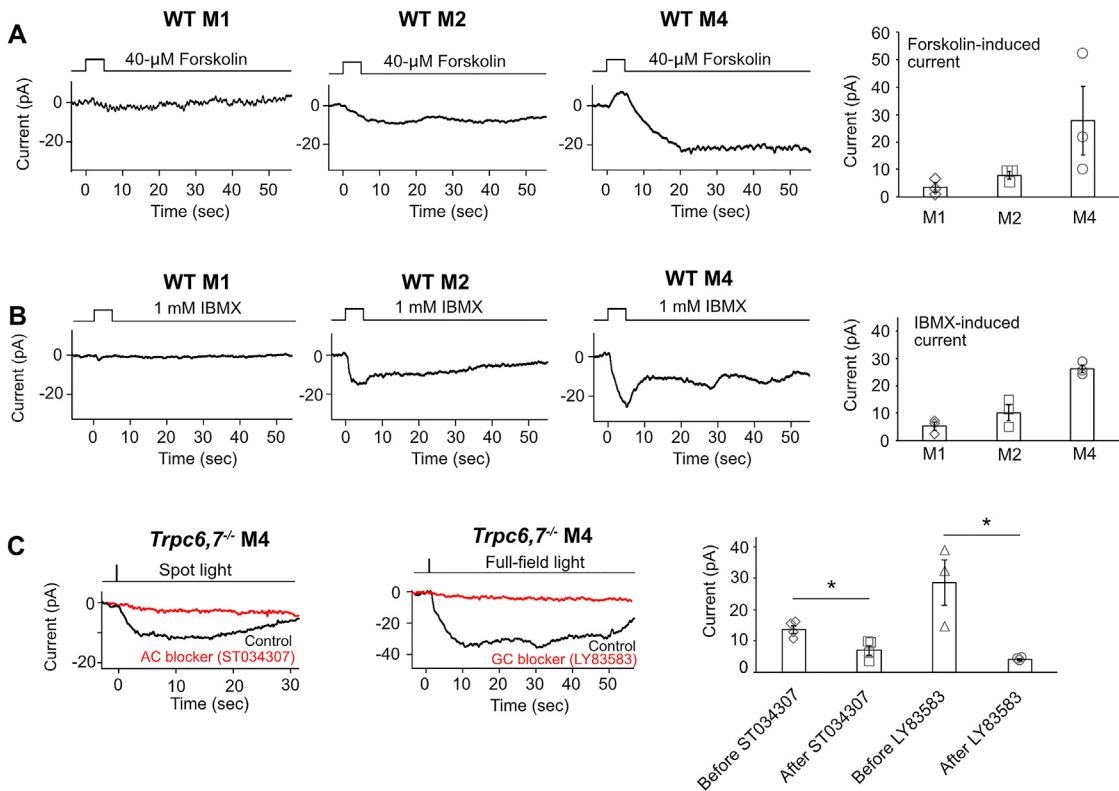


Figure S3. Pharmacological Evidence Indicates Cyclic Nucleotide Pathway Is Involved in the Phototransduction of ipRGCs, Related to Figure 3

(A and B) Puffing 40- μ M Forskolin (adenylyl cyclase activator) or 1 mM IBMX (PDE inhibitor) onto the soma and proximal dendrites of ipRGCs induces current in M2-cells and M4-cells, but has a much smaller effect on M1-cells (mean \pm SEM, n = 3 cells from at least 2 animals in each group). In M4-cells, Forskolin also induces a small outward current prior to the large inward current, which might due to non-specific effect of Forskolin on ion-channels. The representative traces are recorded from different cells.

(C) Left, Bath application of 50- μ M ST034307 (adenylyl cyclase blocker) effectively reduces light response (spot light centered on soma) of *Trpc6,7*^{-/-} M4 cells. Because the blocker may not have completely penetrated within the 30-min recording period, spot light stimulation (40 μ m in diameter) was used to limit melanopsin activation to the soma and proximal dendrites which are exposed to bath solution in a microdissection procedure before recording. Middle, Bath application of 120- μ M LY83583 (guanylyl cyclase blocker) largely reduces light response (full-field) of *Trpc6,7*^{-/-} M4 cells. Right, Collective data of peak photocurrent (mean \pm SEM, n = 4, 4, 3, 3 cells from at least 2 animals in each group. * indicates p < 0.05).

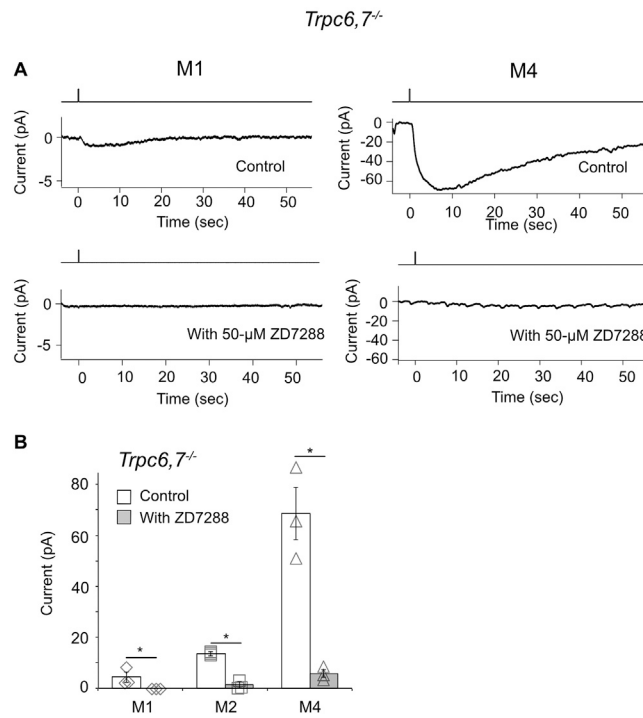


Figure S4. Intrinsic Light Responses of *Trpc6,7^{-/-}* M1- and M4-Cells Were Blocked by Bath Application of 50- μ M ZD7288, Related to Figure 4

(A) Representative traces (see Figure 4 for *Trpc6,7^{-/-}* M2-cell).

(B) Collective results of M1-, M2- and M4-cells (mean \pm SEM, n = 3 cells from at least 2 animals in each group. * indicates being statistically significant, $p < 0.05$). A small oscillation of the membrane current in M2 or M4 cell in the presence of ZD7288 was sometimes observed.

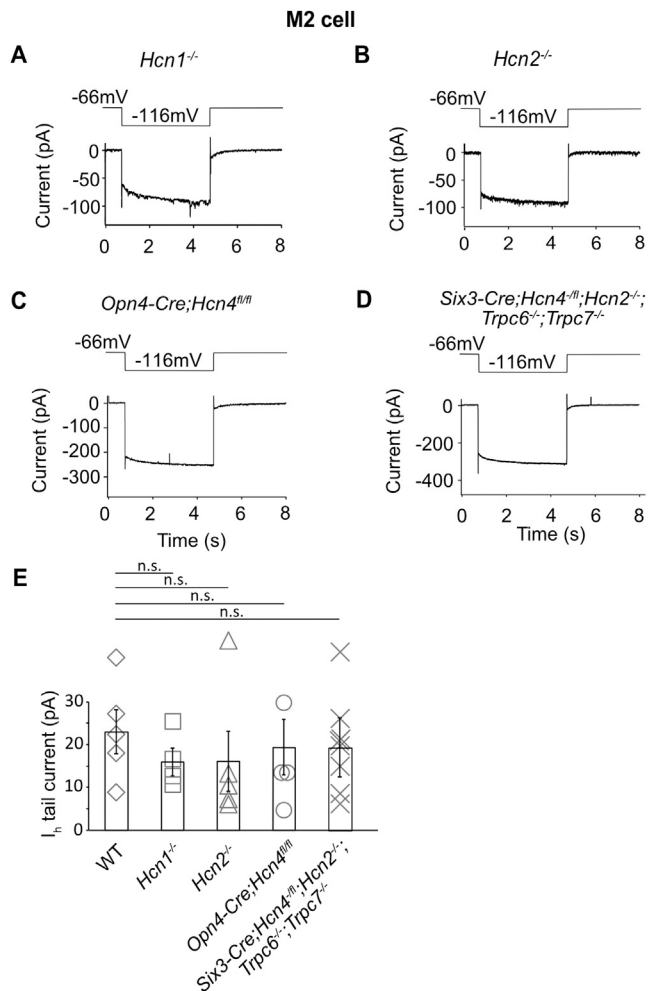


Figure S5. I_h Tail Currents in *Hcn1*^{-/-}, *Hcn2*^{-/-}, *Opn4-Cre;HCN4*^{fl/fl}, and *Six3-Cre;Hcn4*^{fl/fl}; *Hcn2*^{-/-}; *Trpc6*^{-/-}; *Trpc7*^{-/-} M2-Cells Had Normal Amplitudes, Related to Figure 5

(A–D) Representative traces. I_h tail current was induced by a 4-s hyperpolarization to -116 mV before returning to -66 mV (see text).

(E) Collective data of I_h tail current (mean \pm SEM, $n = 5, 4, 5, 4, 8$ cells from at least 2 animals in each group; n.s. indicates no significant difference, $p > 0.05$). We speculate that the negative results (unchanged I_h tail currents) on *Opn4-Cre;HCN4*^{fl/fl} and *Six3-Cre;Hcn4*^{fl/fl}; *Hcn2*^{-/-}; *Trpc6*^{-/-}; *Trpc7*^{-/-} M2-cells were probably due to the difficulty in inducing recombination of the particular *Hcn4*-floxed allele (see text).

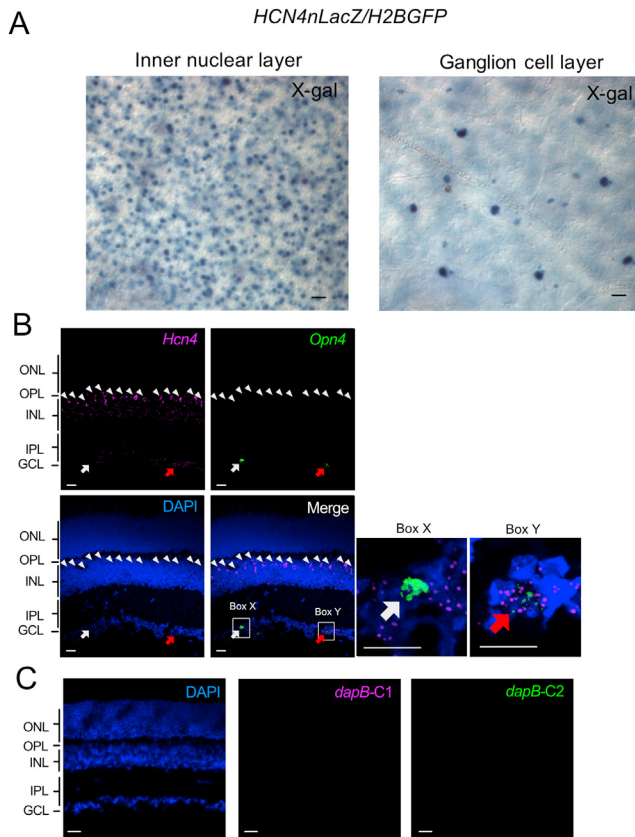


Figure S6. *Hcn4* mRNA Is Expressed in Mouse Retinal Ganglion Cell Layer and Partially Co-localized with *Opn4* mRNA, Related to Figure 5

(A) Positive X-gal staining (substrate of β-Gal coded by *LacZ*) of *HCN4nLacZ/H2BGFP* (see text) whole-mount mouse retina in the absence of Cre-recombinase to demonstrate the validity of the *HCN4nLacZ/H2BGFP* mouse line. X-gal signal (blue) was found in inner nuclear layer (left), known to contain HCN4-expressing bipolar cells (Mataruga et al., 2007), as well as in the ganglion cell layer (right).

(B) Co-expression pattern of *Opn4* and *Hcn4* mRNA in mouse retinal section revealed by *in situ* hybridization (RNAscope, ACD). White arrow: an example of a dense *Opn4*-mRNA cluster with few nearby *Hcn4* mRNA (possibly an M1-cell); red arrow: an example of a sparse *Opn4*-mRNA cluster with abundant *Hcn4* mRNA in close proximity (possibly an M2 or M4-cell). Boxed areas in the merged image are magnified in boxes X and Y. *Hcn4* mRNA is also detected in the inner nuclear layer, presumably HCN4-expressing bipolar cells (arrowheads, see also (A)).

(C) No fluorescence signal was detected with negative control probes (*dapB-C1* and *dapB-C2*) targeting a bacterial gene (*dapB*). ONL, outer nuclear layer; OPL, outer plexiform layer; INL, inner nuclear layer; IPL, inner plexiform layer; GCL, ganglion cell layer. Scale bar, 20 μm.